2014

Discovery of lead compounds targeting the bacterial sliding clamp using a fragment-based approach

Zhou Yin
University of Wollongong, zy877@uowmail.edu.au

Louise Whittell
University of Wollongong, lwhittel@uow.edu.au

Yao Wang
University of Wollongong, yw974@uowmail.edu.au

Slobodan Jergic
University of Wollongong, jergic@uow.edu.au

Michael Liu
University of Technology, Sydney

See next page for additional authors

Publication Details

Yin, Z., Whittell, L. R., Wang, Y., Jergic, S., Liu, M., Harry, E. J., Dixon, N. E., Beck, J. L., Kelso, M. J. & Oakley, A. J. (2014). Discovery of lead compounds targeting the bacterial sliding clamp using a fragment-based approach. Journal of Medicinal Chemistry, 57 (6), 2799-2806.

Discovery of lead compounds targeting the bacterial sliding clamp using a fragment-based approach

Abstract
The bacterial sliding clamp (SC), also known as the DNA polymerase III β subunit, is an emerging antibacterial target that plays a central role in DNA replication, serving as a protein–protein interaction hub with a common binding pocket to recognize linear motifs in the partner proteins. Here, fragment-based screening using X-ray crystallography produced four hits bound in the linear-motif-binding pocket of the *Escherichia coli* SC. Compounds structurally related to the hits were identified that inhibited the *E. coli* SC and SC-mediated DNA replication in vitro. A tetrahydrocarbazole derivative emerged as a promising lead whose methyl and ethyl ester prodrug forms showed minimum inhibitory concentrations in the range of 21–43 μg/mL against representative Gram-negative and Gram-positive bacteria species. The work demonstrates the utility of a fragment-based approach for identifying bacterial sliding clamp inhibitors as lead compounds with broad-spectrum antibacterial activity.

Keywords
CMMB

Disciplines
Medicine and Health Sciences | Social and Behavioral Sciences

Publication Details
Yin, Z., Whittell, L. R., Wang, Y., Jergic, S., Liu, M., Harry, E. J., Dixon, N. E., Beck, J. L., Kelso, M. J. & Oakley, A. J. (2014). Discovery of lead compounds targeting the bacterial sliding clamp using a fragment-based approach. Journal of Medicinal Chemistry, 57 (6), 2799-2806.

Authors
Zhou Yin, Louise Whittell, Yao Wang, Slobodan Jergic, Michael Liu, Elizabeth J. Harry, Nicholas Dixon, Jennifer Beck, Michael Kelso, and Aaron Oakley

Discovery of Lead Compounds Targeting the Bacterial Sliding Clamp using a Fragment-Based Approach

Zhou Yin,[†] Louise R. Whittell,[†] Yao Wang,[†] Slobodan Jergic,[†] Michael Liu,[‡] Elizabeth J. Harry,[‡] Nicholas E. Dixon,[†] Jennifer L. Beck,[†] Michael J. Kelso,[†] and Aaron J. Oakley*,[†]

[†]School of Chemistry and Centre for Medical and Molecular Bioscience, University of Wollongong, New South Wales, Australia.

[‡]ithree Institute, University of Technology, Sydney, New South Wales, Australia

ABSTRACT: The bacterial sliding clamp (SC), also known as the DNA polymerase III β subunit, is an emerging antibacterial target that plays a central role in DNA replication, serving as a protein–protein interaction hub with a common binding pocket to recognize linear motifs in the partner proteins. Here, fragment-based screening using X-ray crystallography produced four hits bound in the linear-motif-binding pocket of the *Escherichia coli* SC. Compounds structurally related to the hits were identified that inhibited the *E. coli* SC and SC-mediated DNA replication *in vitro*. A tetrahydrocarbazole derivative emerged as a promising lead whose methyl and ethyl ester prodrug forms showed minimal inhibitory concentrations in the range of 21–43 μg/mL against representative Gram-negative and Gram-positive bacteria species. The work demonstrates the utility of fragment-based approach for identifying bacterial sliding clamp inhibitors as lead compounds with broad-spectrum antibacterial activity.

INTRODUCTION

The emergence of antibiotic-resistant bacteria has presented a great challenge to humanity[1] with new classes of antibiotics acting on novel targets being urgently needed.[2-4] The bacterial sliding clamp (SC), also known as the DNA polymerase III (Pol III) β subunit, is a torus-shaped homodimeric protein[5] that is conserved across bacterial species.[6-8] The SC serves as a protein–protein interaction (PPI) hub during bacterial DNA replication and repair,[9, 10] surrounding double-stranded DNA and subsequently recruiting a diverse range of protein binding partners, including the δ and α subunits of DNA Pol III, DNA Pols I, II, IV, V and MutS.[5, 9] The pivotal role it plays in bacterial DNA replication and repair, its conserved structure across bacterial species[6-8] and its structural divergence from the equivalent human protein (proliferating cell nuclear antigen, PCNA)[9, 11] make the SC a highly attractive target for producing new antibiotics acting via a novel mechanism.

Proteins that interact with the SC recognise a surface binding pocket that consists of two subsites (I and II),[6, 12, 13] with one pocket located on each of the SC monomers (Figure 1). These protein binding partners interact with the SC using linear motifs (LMs) located on their surfaces.[5, 13, 14] LMs are short (4–10 residue), intrinsically disordered sequences most often found at the termini of proteins but sometimes in loop regions.[15-17] Binding of LMs to rigid protein domains represents a distinct category of protein–protein interactions (PPIs) that generally display weak affinities (K_d ~ 1–100 μM).[18-23] PPIs are attractive drug targets, but the development of small-molecule inhibitors is considered challenging due in part to the shape and large surface areas of such sites.[24] Nevertheless, an increasing number of inhibitors of PPIs are being reported, with recent examples including inhibitors of clathrin,[25] the polo-box domain of polo-like kinase 1[26] and 14-3-3 protein[27].

A consensus LM sequence QLx_1Lx_2F/L (S/D preferred at x_1; x_2 may be absent) has been identified that interacts with the SC LM-binding pocket, and isolated peptides based on this sequence have been shown to bind the SC (Figure 1A) with affinities similar to their parent proteins[28-30] and, conversely, when LMs are removed from the parent proteins, they lose all SC affinity.[13, 31] Our recent work proposed a mechanism of sequential binding of LMs to the *E. coli* SC and highlighting the role of subsite I as the "anchor site" for LM recognition.[30] Two classes of small molecules have previously been reported that bind to subsite I (K_i >10 μM), but no antibacterial activities were provided for these compounds.[12, 28]

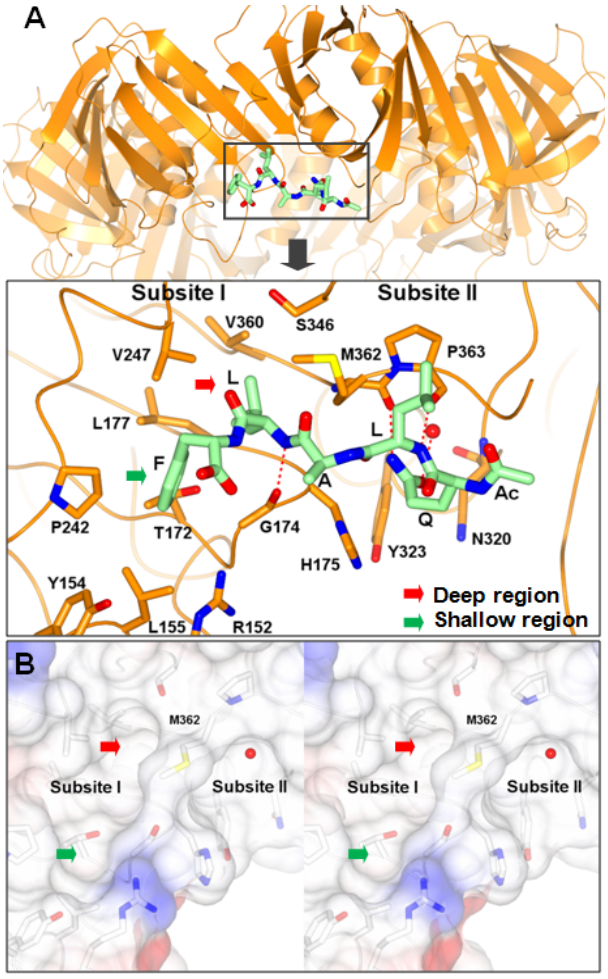

Figure 1. (A) X-ray crystal structures of consensus pentapeptide AcQLALF bound to the *E. coli* SC (PDB entry 4K3P[30]). The complex is shown with the SC colored orange and the peptide carbon atoms light green. All other atoms are presented in CPK colors. Dashed lines in red represent H-bonds. (B) Stereo view of the SC binding pocket (PDB entry 4K3S[30] chain A). SC carbon atoms are shown shaded white. All other atoms are presented in CPK colors. Electrostatic potential surfaces of the binding site are shown with blue = positive and red = negative. A crystallographic water molecule is shown as a red sphere; arrows indicate the deep (red) and shallow (green) regions of subsite I in A and B.

In this work, X-ray crystallography was used as a primary screen to identify fragment hits against the *E. coli* SC. Binding poses adopted by these hits were used in combination with chemo-informatics to guide subsequent inhibitor design, with several promising compounds being identified that bind to the SC, disrupt LM–SC interactions and inhibit SC-dependent DNA replication *in vitro*. Anti-bacterial activity was demonstrated for a lead inhibitor against two Gram negative and two Gram positive bacterial species.

RESULTS

Fragment-Based Screening Using X-Ray Crystallography. A total of 352 fragment compounds from the First Pass Screen (Zenobia Fragment Libraries) were soaked into *E. coli* SC crystals as 4-in-1 cocktails and screened using X-ray crystallography. Four fragment hits showing good electron density: 3,4-difluorobenzamide **1**, 5-chloroisatin **2**, 6-nitrobenzopyrazole **3** and 5-nitroindole **4**, were found to bind in subsite I of the binding pocket on Chain A of the SC dimer (complexes denoted as SC^1, SC^2, SC^3 and SC^4, respectively, in Figure 2; crystallographic data are in Table S1, Supporting Information). No significant changes in the SC main-chain structure were observed upon fragment binding. Several other fragments were identified that bind in subsite I but they showed only weak electron density and were not investigated further. An additional six fragments were identified that bound only in the binding pocket of chain B, where they were stabilized by a symmetry-related protein molecule. These were considered to be crystallographic artefacts and were not pursued.

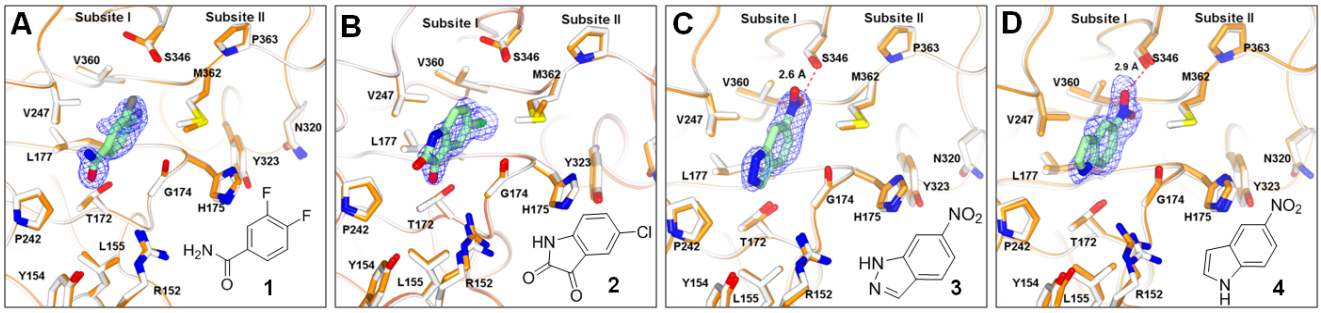

Figure 2. X-ray co-crystal structures showing binding of fragment hits **1**–**4** to subsite I of the *E. coli* SC LM-binding pocket. The complexes denoted (A) SC^1, (B) SC^2, (C) SC^3 and (D) SC^4 are shown with the SC carbon atoms colored orange and the bound fragment carbon atoms light green. All other atoms are presented in CPK colors. *Apo*-SC structures (PDB entry 4K3S[30] chain A) are superimposed on the SC structures in the complexes for comparison (shown in white). Hydrogen bonds from S346 to fragment nitro-groups are represented as dashed red lines. Electron density maps ($2mF_o$–DF_c) contoured at 1 σ are shown in blue wire-basket form.

The four fragment hits bound in the deep region of subsite I forming van der Waals' interactions with the hydrophobic side chains of V360, V247, L177 and M362 (Figure 2). The shallow region of subsite I, comprising residues T172, P242 and L155, remained vacant (Figures 1B and 2). Each fragment positioned an aromatic ring in the narrow groove of subsite I with the fluoro and chloro substituents of **1** and **2** being buried in the deep hydrophobic region (Figure 2A,B). Binding of both **1** and **2** caused rotation of the side chain of S346 relative to the *apo*-SC structure. Fragments **3** and **4** bound in a similar manner to **1** and **2** placing their NO_2 groups in the positions occupied by the halogen atoms of **1** and **2** (Figure 2C,D). The NO_2 groups appeared to accept H-bonds from the side-chain of S346, allowing this residue to retain the same conformation it

adopts in the *apo*-SC structure.[30]

A fluorescence polarization (FP)-based competition assay was used to quantify inhibition of a LM–SC interaction by the four fragment hits.[30] In this assay, a fluorescently labeled SC-binding tracer peptide based on a LM derived from the consensus-binding motif (5-carboxyfluorescein-QLDLF, K_d = 70 nM)[12, 32, 33] was used as the competitive probe ligand. Inhibition of tracer binding to the *E. coli* SC was plotted against inhibitor concentrations and IC_{50} values were calculated and transformed into inhibition constants (K_i) using the Kenakin correction for ligand depletion.[34] None of the four hits **1**–**4** showed any significant inhibition of probe binding below 1 mM under the assay conditions (data not shown).

Identification of Fragments That Fully Occupy Subsite I. Following identification of fragment hits **1**–**4**, we sought to improve binding affinity by identifying fragments that could more completely occupy subsite I, including the shallow region. It was noted that the fluoroaryl ring found in **1** was also present in the previously reported biphenyl inhibitor[28], triggering further investigations with compound **5**,a readily available analogue containing the fluorobiphenyl moiety (Table 1). A K_i of 280 μM was measured for **5** using the FP assay[30] (Table 1) and its X-ray co-crystal structure was solved in complex with the SC (denoted SC^5). Compound **5** was found to fully occupy subsite I (Figure 3A; crystallographic data in Table S2, Supporting Information), with its fluoroaryl ring adopting a similar binding pose to that of **1**. The side-chain of M362 was observed to rotate toward subsite II, possibly due to steric crowding. The second phenyl ring of **5** occupied the shallow region of subsite I, with its carboxylate group involved in a salt bridge and/or H-bonds with the side chains of R152 and Y154. Both of these side chains move slightly toward the carboxylate of **5** relative to their positions in the *apo*-structure.

The ZINC library[35] was subsequently searched for compounds displaying structural similarity to fragments **1**–**5**. Selected molecules were subjected to a docking-based screen using UCSF DOCK6.5[36] and candidates were purchased for screening using the FP assay. Initial efforts failed to yield hits with K_i < 1 mM but it was noted during the work that 5-chlorocarbazoles appeared promising. Further searches of the ZINC library[35] identified several 5-chlorocarbazoles including **6**, which showed a K_i of 199 μM (Table 1 and Table S3, Supporting Information). The X-ray co-crystal structure of **6** was obtained, but the compound, although clearly binding in subsite I, showed only weak electron density (data not shown).

The slight curvature at the base of subsite I (due to P242) appeared likely to impair binding of rigid/planar compounds like **6** and it was postulated that ligands with increased flexibility might better complement the curvature. Searches of the ZINC library[35] (Table S3, Supporting Information) identified tetrahydrocarbazoles **7** and **8**, which were found to have K_i values of 216 and 64 μM, respectively (Table 1). Compounds **9** and **10**, the methyl and ethyl esters of **8**, displayed significantly weaker

binding, highlighting the importance of the acid group. Eighteen additional tetrahydrocarbazoles were synthesized and evaluated using the FP assay but all showed poor SC binding affinities (**11**–**29**, Table S3 and Scheme S1, Supporting Information).

The X-ray co-crystal structures of **7** and **8** in complex with the *E. coli* SC were solved (denoted as SC^7 and SC^8 in Figure 3B,C; crystallographic data in Table S2, Supporting Information). Compounds **7** and (*R*)-**8** were both found to completely occupy subsite I with their tetrahydrocarbazole rings nestled against P242. Binding of **7** preserved the position of all residues in subsite I and had no effect on the overall protein structure. The carboxylate group of **7** made two H-bonds to the backbone carbonyl oxygen atom of V247 and the hydroxyl group of S346. Interestingly, while the commercially obtained carboxy-5-chlorotetrahydrocarbazole **8** was racemic only the (*R*)-enantiomer appeared in the electron density map (Figure 3C). The binding of (*R*)-**8** caused conformation changes in the M362 and S346 side chains relative to the *apo*-structure and buried the 5-chloro group in the hydrophobic deep region of subsite I. The carboxyl group of **8** appeared to interact with the guanidinium group of R152, which may explain the preference for binding of the (*R*)-enantiomer in the crystal.

Ligand efficiency (LE) and ligand lipophilicity efficiency (LLE_{AT})[37] were calculated (Supporting Information) to assess the suitability of these fragments for further medicinal chemistry optimization (Table 1), where it is considered that compounds with LE and LLE_{AT} values greater than 0.3 are desirable.[37] Compounds **7** and **8** showed LLE_{AT} values > 0.4 suggesting they are attractive scaffolds for further optimization.

Table 1. Follow-up Fragment Inhibitors of the *E. coli* SC Identified from Initial Hits 1–4

Compound	Structure	IC_{50} (μM)	K_i (μM)	LE (kcal/mol)	LogD (pH 7.2)	LLE_{AT}
5	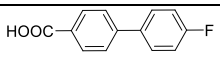	504	280	0.3	–3.17	0.22
6	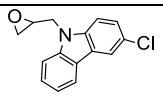	358	199	0.28	–4.93	0.12

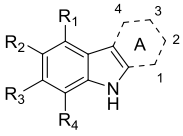

Compound	R_1	R_2	R_3	R_4	Ring A	IC_{50} (μM)	K_i (μM)	LE (kcal/mol)	LogD (pH 7.2)	LLE_{AT}
7	H	Cl	CO_2H	H	cyclohexyl	389	216	0.3	–0.48	0.45
8	H	Cl	H	H	1-CO_2H cyclohexyl	115	64	0.34	0.36	0.42
9	H	Cl	H	H	1-CO_2Me cyclohexyl	> 1000	n/a	n/a	n/a	n/a
10	H	Cl	H	H	1-CO_2Et cyclohexyl	~ 899	~ 499	0.24	4.44	0.03

n/a: not available

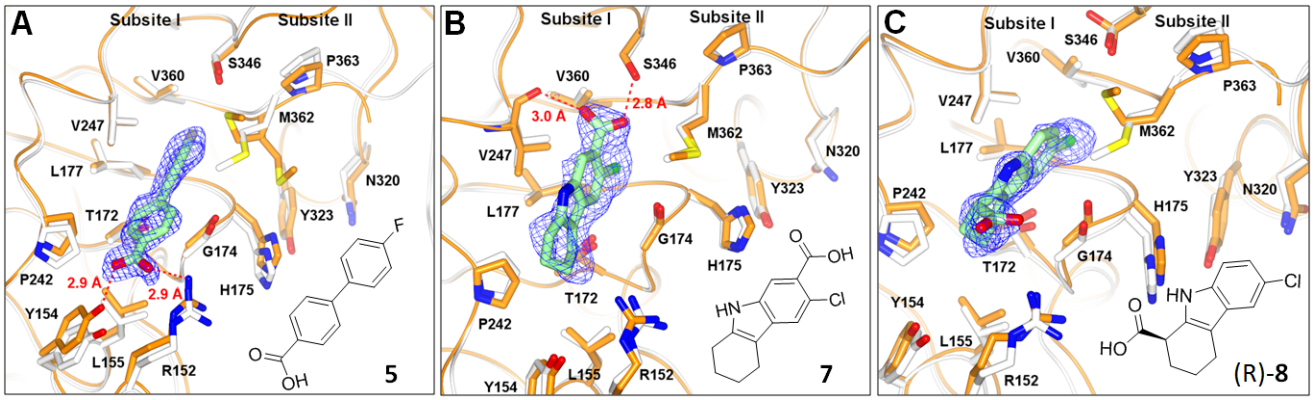

Figure 3. X-ray co-crystal structures of **5**, **7** and **8** bound to subsite I of the *E. coli* SC LM-binding pocket. Complexes are denoted (A) SC[5], (B) SC[7], (C) SC[8] and are shown with the SC carbon atoms colored orange and the ligand carbon atoms light green. All other atoms are presented in CPK colors. *Apo*-SC structures (PDB entry 4K3S[30] Chain A in B and 1MMI[38] Chain A in A and C) are superimposed (shown in white) on the SC structures of the complexes for comparison. H-bonds are represented as dashed red lines. Electron density maps ($2mF_o$–DF_c) contoured at 1 σ are shown in blue wire-basket form.

Two *E. coli* SC inhibitors, a thioxothiazolidinyl derivative RU7 [12] and a biphenyloxime ether derivative,[28] have previously been identified that bind to the subsite I. Their binding poses are compared with that of (*R*)-**8** in Figure S1 (Supporting Information). It is noteworthy that when superimposed, the aryl ring systems of all three compounds are approximately co-planar and project their halogens into the deep region of subsite I (Figure 1B). While all three compounds show low-micromolar affinity, RU7 and the biphenyloxime ether derivative project large moieties towards bulk solvent that appear to contribute few (if any) binding interactions. In the case of RU7, the thiocarbonyl and carboxymethyl moieties are oriented toward solvent while the biphenyloxime ether derivative projects its substituted cyclohexyl moiety toward the solvent. Compound (*R*)-**8**, on the other hand, projects no groups out into the solvent and better complements the geometry of subsite I, thus suggesting it is a more suitable lead for optimization studies.

***E. coli* SC Inhibitors Disrupt *in vitro* DNA Replication and show Antibacterial Effects.** An *in vitro* DNA replication assay was used to assess inhibition of *E. coli* SC function by compounds **5**–**8**. The reaction system contained the SC, Pol III α subunit and the reconstituted clamp loader complex ($\gamma_3\delta\delta'$).[39] During *E. coli* replication the SC is loaded onto DNA by the clamp-loader complex (composed minimally of Pol III δ, γ/τ and δ' subunits)[40-42] and confers high processivity upon the Pol III α subunit (the replicase) by acting as a mobile tether.[43, 44] Circular single-stranded M13 DNA (ssDNA) with an annealed RNA primer was used as the template for DNA synthesis and was coated with single-stranded DNA-binding protein (SSB). The SC is loaded onto the primed DNA by the clamp loader complex and the α subunit (bound to the SC) catalyzes extension of the primer through incorporation of dNTPs using ssDNA as a template. A schematic illustration of this assay is shown in the Supporting Information (Figure S3).

With this assay system, binding of the DNA Pol III δ and α subunits to the SC is essential for replication, meaning impaired SC binding due to the presence of inhibitors will hinder DNA synthesis, as shown by the presence of ssDNA templates and incomplete dsDNA products. A complete dsDNA product is formed when the whole of the ssDNA circle is replicated (see Figure S4, Supporting Information for control experiment). Compounds **5**, **6** and **7** were found to inhibit replication at 500 or 1000 μM (Figure 4A–C), while compound **8** produced complete inhibition at 250 μM (Figure 4D), consistent with its higher SC affinity (Table 1).

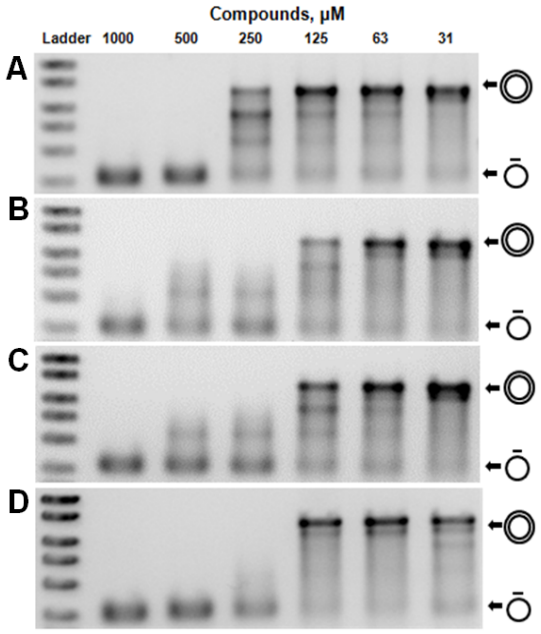

Figure 4. Inhibition of SC-dependent *in vitro* DNA synthesis by **5** (A), **6** (B), **7** (C) and **8** (D). Ladders on the left show molecular size markers. Circles with a dash above represent primed ssDNA templates and concentric circles represent fully replicated dsDNA product.

The antibacterial effects of compounds **5, 7–10** were carried out against two representative Gram-negative (*E. coli* and *A. baylyi*) and two Gram-positive (*B. subtilis* and *S. aureus*) species. The background-corrected optical density was measured after 24 hours of bacterial growth (Table S4, Supporting Information). The minimum inhibitory concentrations (MICs), defined as the background-corrected optical densities of less than 0.1, are shown in Table 2. Compounds **5** and **7** showed only slight antibacterial activity (MICs 540 to 1246 μg/mL), consistent with their modest *E. coli* SC-binding affinities (Table 1). Their carboxylic acid groups may have reduced membrane penetration. The MIC of **8** (39–78 μg/mL) was lower than **5** and **7** against all four species, consistent with its higher SC affinity (Table 1). Compounds **9** and **10** were considered as possible prodrug forms of **8** (i.e., methyl and ethyl esters, respectively) that might show improved membrane penetration properties. Esters **9** and **10** displayed increased antibacterial activity relative to **8** (MICs 21–43 μg/mL) despite having lower affinities for the SC (Table 1), consistent with their acting as membrane permeable prodrugs.

Table 2. Antibacterial Activities of Compounds 5–10

Compound	Minimum inhibitory concentration (MIC)							
	E. coli		*A. baylyi*		*B. subtilis*		*S. aureus*	
	μM	μg/mL	μM	μg/mL	μM	μg/mL	μM	μg/mL
5	2500	540	5000	1080	2500	540	5000	1080
7	2500	623	5000	1246	2500	623	2500	623
8	313	78	313	78	156	39	156	39
9	156	41	78	21	78	21	156	41
10	78	22	156	43	78	22	78	22

n/a: not available

DISCUSSION

PPIs are often considered difficult targets to inhibit with small molecules.[45] Nevertheless, several PPI inhibitors have been successfully developed.[46] Studies indicate that PPIs rely on so-called "hotspots" for most of the interaction energy and, accordingly, these are usually the most productive sites for inhibitor design.[24] We previously identified subsite I as the "anchor site" of consensus peptide binding to the *E. coli* SC, indicating that this site acts as the SC "hotspot".[30] We also showed that the affinity of peptide LMs for the *E. coli* SC arises from residues occupying both subsites I and II,[30] suggesting that the potential of these individual subsites as drug targets is probably limited. The close proximity of the two subsites, however, suggests that fragment-based approaches are highly suited to identifying inhibitors of this target.

Fragment screening in the current work using X-ray crystallography initially identified four hits, but these proved to be weak binders (K_i >1 mM). The high sensitivity of X-ray crystallography and its ability to identify weak binders in fragment-based screening efforts has previously been noted.[47]

All four hits were found to bind in subsite I, i.e., the LM "anchor site".[30] Follow-up investigations led to the identification of several SC-binding ligands with the substituted tetrahydrocarbazole **8** showing the highest SC affinity (K_i = 64 μM) and excellent ligand lipophilicity efficiency (LLE_{AT} = 0.42). Tetrahydrocarbazoles **7** and **8** were shown by crystallography to bind in subsite I and to inhibit *in vitro* DNA replication. Although compound **8** showed antibacterial activity (MICs 39–78 μg/mL) against representative bacteria, these effects were improved upon masking the carboxylic acid as methyl and ethyl ester prodrugs (compounds **9** and **10**, MICs 21–43 μg/mL). In this study the X-ray crystallography screening, and FP and *in vitro* DNA replication assays were all carried out using the SC from *E. coli*, yet similar antibacterial potencies were observed with

compounds **9** and **10** against *E. coli*, *A. baylyi*, *B. subtilis* and *S. aureus*. This finding is consistent with the high conservation of SC structure across bacterial species[6] and suggests that the *E. coli* SC serves as an excellent model system for identifying SC inhibitors that could potentially be developed into broad-spectrum antibiotics.

Current work in our laboratories aims to improve the SC affinities of the tetrahydrocarbazoles by targeting both subsite I and II. Our previous work suggested that residues of peptide ligands occupying subsite II contribute significantly to the binding affinity and that binding at subsite II is subsequent to binding at subsite I (the "anchor site").[30] A conformational change in the side chain of M362 was proposed to act as a gate in the channel region connecting subsite I and II.[30] A similar conformational change in M362 was observed with the binding of (*R*)-**8** in subsite I (Figure 3C). Therefore the synthesis of tetrahydrocarbazole derivatives substituted at the nitrogen atom may expand the inhibitor-binding area beyond subsite I, into the channel region and subsite II.

Materials and Methods

Compounds. Fragment compounds (including **1–4**) were purchased from Zenobia Therapeutics (First-Pass Screen library). Compounds **5–10** and **6a–c** were purchased from Sigma-Aldrich, Labotest, Enamine or Vitas-M Laboratory. Purchased compounds were $\geq$ 95% pure as confirmed by proton NMR and/or LC-MS. Compounds **11–29** (Table S3, Supporting Information) were synthesized in house (Scheme S1, Supporting Information).

Protein Over-expression and Purification. Expression and purification of the *E. coli* SC, Pol III α subunit, SSB and the clamp loader complex ($\gamma_3\delta\delta'$) were as described previously.[29, 38, 39, 48]

Crystallization and X-Ray Data Collection. Crystals of the *E. coli* SC were grown at 285 K by the hanging-drop vapor diffusion method. The drop was composed of 1 μL of sliding clamp (53 mg/mL) mixed with the same volume of reservoir solution of 100 mM MES pH 6.5, 100–150 mM $CaCl_2$ and 25–30% (v/v) PEG400. The reservoir volume was 1 mL. SC crystal were moved to a $CaCl_2$-free reservoir and ligands were soaked into the crystal at 2–5 mM with < 10% DMSO. Fragment compounds were mixed as 4-in-1 cocktails as suggested by the supplier and soaked into crystals with each fragment at 5 mM. All crystals were mounted using MiTeGen™ loops on pins with magnetic caps. For in-house data collection crystals were flash-frozen at 100 K using an Oxford Cryo-stream. Diffraction data were collected using a MAR345 desktop beamline using CuKα X-rays from a Rigaku 007HF rotating anode generator with Varimax™ optics. For synchrotron data collection, the SSRL Automated Mounting system (SAM) was used. Mounted crystals were flash-frozen in

liquid nitrogen and diffraction data were collected at the Australian Synchrotron, Beamline MX1 (X-ray wavelength 0.95 Å) using Blu-Ice.[49]

Data Processing, Structure Solution and Refinement. Crystal data sets were integrated, merged and scaled with either HKL2000[50] or MOSFLM and SCALA.[51] The structures were solved by molecular replacement with CCP4 using the Protein Data Bank entry 1MMI or 4K3S as the starting model. Iterative cycles of model building and refinement were performed in COOT[52] and REFMAC5.[53]

Fluorescence Polarization Assay. FP experiments were carried out according to the published protocol.[30]

Molecular Docking and Chemoinformatics. Details are in Supporting Information.

Antibacterial Activity. Determination of minimum inhibitory concentrations (MICs) were carried out with bacterial strains *Escherichia coli* DH5α, *Acinetobacter baylyi* ADP1, *Bacillus subtilis* SU5 and *Staphylococcus aureus* NCTC8325. Experiments followed the CLSI broth microdilution method.[54] Briefly, strains were grown overnight and diluted to 5 x 10^4 CFU/mL with cation-adjusted Mueller Hinton II broth and used as inoculated medium for bacterial growth. Serial 2-fold dilution of candidate compounds (pre-dissolved in DMSO at 100 mM) or antibiotics were carried out in sterile 96-well plates. Controls consisted of the growth medium only (blank controls) or inoculated medium with 5% DMSO or DMSO diluted as for the test compounds (negative controls), and inoculated medium with antibiotics (positive controls). Optical density values of each inoculated culture were measured at wavelength 595 nM as the background using a plate reader (Tecan Infinite M200 Pro). The plates were incubated for 24 h at 37°C and then the optical density values of the bacterial culture were measured again. MICs were defined as the lowest compound concentration with background-subtracted optical density < 0.1.

DNA replication assay. Each assay contained 20 mM Tris-HCl pH 7.6, 10 mM $MgCl_2$, 0.8 mM ATP, 8.4 mM dithiothreitol, 0.6 mM of each dNTP, 211 nM Pol III α subunit, 700 nM SSB (as tetramers), 210 nM Pol III β subunit (as dimers), 42 nM $\gamma_3\delta\delta'$ clamp loader complex, 120 mM NaCl and 3 nM RNA primed M13 ssDNA template, in a volume of 6.8 μL. Compounds were dissolved in DMSO and diluted in series 2-fold (in 50% v/v DMSO) before being added (0.5 μL) to the assay mixture at 0°C. The final DMSO concentration was 3.4% (v/v) in all assays. The assay mixtures were treated at 30°C for 60 min before being quenched by the addition of EDTA to 150 mM and SDS to 1% (w/v). The DNA products were separated by 0.7% agarose gel electrophoresis in TAE buffer (80 mM Tris, 40 mM acetic acid, and 4 mM EDTA) and then stained with 10,000-fold diluted SYBR Gold (Invitrogen) for 60 min. The DNA products were visualized using a UV transilluminator.

ASSOCIATED CONTENT

Supporting Information

Crystallographic data, additional chemical and biochemical data and figures, detailed materials and methods. This material is available free of charge via the Internet at http://pubs.acs.org.

Accession Codes

The atomic coordinates and structure factors for SC^{1}, SC^{2}, SC^{3}, SC^{4}, SC^{5}, $SC^{7}$and SC^{8}, have been deposited with the Protein Data Bank under accession codes 4N94, 4N95, 4N96, 4N97, 4N98, 4N99 and 4N9A, respectively.

AUTHOR INFORMATION

Corresponding Author

*Email: aarono@uow.edu.au; phone: +61-42214347

Author Contributions

A.J.O., M.J.K., N.E.D., E.H., and J.L.B. supervised the project. Z.Y. performed the fluorescence polarization-based assays, molecular docking and chemoinformatics studies. Z.Y and A.J.O performed X-ray crystallography. Antibacterial testing was performed by Z.Y and M.L. Organic syntheses were performed by L.R.W. Replication assays were performed by Y.W. and S.J. The manuscript was initially drafted by Z.Y., L.R.W. and Y.W. with input from all co-authors.

ACKNOWLEDGMENTS

Parts of this research were undertaken on the MX1 beamline at the Australian Synchrotron, Victoria, Australia. This research was supported by an Australian Research Council Discovery Project (DP110100660) and Future Fellowship (FT0990287) to A.J.O.

ABBREVIATIONS USED

dNTP, deoxyribonucleoside triphosphate; dsDNA, double-stranded DNA; FP, fluorescence polarization; IC_{50}, half-maximum inhibitory concentration; K_i, inhibition constant; LC-MS, Liquid chromatography–mass spectrometry; LogD, distribution coefficient; LE, Ligand efficiency; LLE_{AT}, ligand lipophilicity efficiency; LM, linear motif; MIC, minimum inhibitory concentration; NMR, nuclear magnetic resonance; PCNA, proliferating cell nuclear antigen; PDB, protein data bank; Pol, polymerase; PPI, protein–protein interaction; SC, sliding clamp; ssDNA, single-stranded DNA.

REFERENCES

(1) Spellberg, B.; Bartlett, J. G.; Gilbert, D. N. The future of antibiotics and resistance. *N. Engl. J. Med.* **2013**, *368*, 299–302.

(2) Coates, A. R. M.; Halls, G.; Hu, Y. Novel classes of antibiotics or more of the same? *Br. J. Pharmacol.* **2011**, *163*, 184–194.

(3) Devasahayam, G.; Scheld, W. M.; Hoffmann, P. S. Newer antibacterial drugs for a new century. *Expert Opin. Investig. Drugs* **2010**, *19*, 215–234.

(4) Moellering, R. C., Jr. Discovering new antimicrobial agents. *Int. J. Antimicrob. Agents* **2011**, *37*, 2–9.

(5) Kong, X.-P.; Onrust, R.; O'Donnell, M.; Kuriyan, J. Three-dimensional structure of the β subunit of E. coli DNA polymerase III holoenzyme: a sliding DNA clamp. *Cell* **1992**, *69*, 425–437.

(6) Burnouf, D. Y.; Olieric, V.; Wagner, J.; Fujii, S.; Reinbolt, J.; Fuchs, R. P. P.; Dumas, P. Structural and biochemical analysis of sliding clamp/ligand interactions suggest a competition between replicative and translesion DNA polymerases. *J. Mol. Biol.* **2004**, *335*, 1187–1197.

(7) Argiriadi, M. A.; Goedken, E. R.; Bruck, I.; O'Donnell, M.; Kuriyan, J. Crystal structure of a DNA polymerase sliding clamp from a Gram-positive bacterium. *BMC Struct. Biol.* **2006**, *6*, 2.

(8) Gui, W. J.; Lin, S. Q.; Chen, Y. Y.; Zhang, X. E.; Bi, L. J.; Jiang, T. Crystal structure of DNA polymerase III β sliding clamp from *Mycobacterium tuberculosis*. *Biochem. Biophys. Res. Commun.* **2011**, *405*, 272–277.

(9) Indiani, C.; O'Donnell, M. The replication clamp-loading machine at work in the three domains of life. *Nat. Rev. Mol. Cell. Biol.* **2006**, *7*, 751–761.

(10) Johnson, A.; O'Donnell, M. Cellular DNA replicases: components and dynamics at the replication fork. *Annu. Rev. Biochem.* **2005**, *74*, 283–315.

(11) López de Saro, F. J.; Georgescu, R. E.; Goodman, M. F.; O'Donnell, M. Competitive processivity-clamp usage by DNA polymerases during DNA replication and repair. *EMBO J.* **2003**, *22*, 6408–6418.

(12) Georgescu, R. E.; Yurieva, O.; Kim, S. S.; Kuriyan, J.; Kong, X. P.; O'Donnell, M. Structure of a small-molecule inhibitor of a DNA polymerase sliding clamp. *Proc. Natl. Acad. Sci. U.S.A.* **2008**, *105*, 11116–11121.

(13) Dalrymple, B. P.; Kongsuwan, K.; Wijffels, G.; Dixon, N. E.; Jennings, P. A. A universal protein-protein interaction motif in the eubacterial DNA replication and repair systems. *Proc. Natl. Acad. Sci. U.S.A.* **2001**, *98*, 11627–11632.

(14) Shamoo, Y.; Steitz, T. A. Building a replisome from interacting pieces: sliding clamp complexed to a peptide from DNA polymerase and a polymerase editing complex. *Cell* **1999**, *99*, 155–166.

(15) Fong, J. H.; Shoemaker, B. A.; Garbuzynskiy, S. O.; Lobanov, M. Y.; Galzitskaya, O. V.; Panchenko, A. R. Intrinsic disorder in protein interactions: insights from a comprehensive structural analysis. *PLoS Comput. Biol.* **2009**, *5*, e1000316.

(16) Meszaros, B.; Tompa, P.; Simon, I.; Dosztányi, Z. Molecular principles of the interactions of disordered proteins. *J. Mol. Biol.* **2007**, *372*, 549–561.

(17) Gould, C. M.; Diella, F.; Via, A.; Puntervoll, P.; Gemund, C.; Chabanis-Davidson, S.; Michael, S.; Sayadi, A.; Bryne, J. C.; Chica, C.; Seiler, M.; Davey, N. E.; Haslam, N.; Weatheritt, R. J.; Budd, A.; Hughes, T.; Pas, J.; Rychlewski, L.; Trave, G.; Aasland, R.; Helmer-

Citterich, M.; Linding, R.; Gibson, T. J. ELM: the status of the 2010 eukaryotic linear motif resource. *Nucleic Acids Res.* **2010**, *38*, D167–D180.

(18) Pawson, T.; Nash, P. Assembly of cell regulatory systems through protein interaction domains. *Science* **2003**, 300, 445–452.

(19) Puntervoll, P.; Linding, R.; Gemünd, C.; Chabanis-Davidson, S.; Mattingsdal, M.; Cameron, S.; Martin, D. M.; Ausiello, G.; Brannetti, B.; Costantini, A.; Ferrè, F.; Maselli, V.; Via, A.; Cesareni, G.; Diella, F.; Superti-Furga, G.; Wyrwicz, L.; Ramu, C.; McGuigan, C.; Gudavalli, R.; Letunic, I.; Bork, P.; Rychlewski, L.; Küster, B.; Helmer-Citterich, M.; Hunter, W. N.; Aasland, R.; Gibson, T. J. ELM server: A new resource for investigating short functional sites in modular eukaryotic proteins. *Nucleic Acids Res.* **2003**, *31*, 3625–3630.

(20) Stein, A.; Pache, R. A.; Bernado, P.; Pons, M.; Aloy, P. Dynamic interactions of proteins in complex networks: a more structured view. *FEBS J.* **2009**, *276*, 5390–5405.

(21) Nooren, I. M.; Thornton, J. M. Diversity of protein–protein interactions. *EMBO J.* **2003**, *22*, 3486–3492.

(22) Dyson, H. J.; Wright, P. E. Intrinsically unstructured proteins and their functions. *Nat. Rev. Mol. Cell. Biol.* **2005**, *6*, 197–208.

(23) Diella, F.; Haslam, N.; Chica, C.; Budd, A.; Michael, S.; Brown, N. P.; Trave, G.; Gibson, T. J. Understanding eukaryotic linear motifs and their role in cell signaling and regulation. *Front. Biosci.* **2008**, *13*, 6580-6603.

(24) Silvian, L.; Enyedy, I.; Kumaravel, G. Inhibitors of protein–protein interactions: New methodologies to tackle this challenge. *Drug Discov. Today Technol.* **2013**, *10*, e509–e515.

(25) Macgregor, K. A.; Robertson, M. J.; Young, K. A.; von Kleist, L.; Stahlschmidt, W.; Whiting, A.; Chau, N.; Robinson, P. J.; Haucke, V.; McCluskey, A. Development of 1,8-naphthalimides as clathrin inhibitors. *J. Med. Chem.* **2013**, DOI: 10.1021/jm4015263.

(26) Yin, Z.; Song, Y.; Rehse, P. H. Thymoquinone blocks pSer/pThr recognition by Plk1 Polo-box domain as a phosphate mimic. *ACS Chem. Biol.* **2013**, *8*, 303–308.

(27) Thiel, P.; Roglin, L.; Meissner, N.; Hennig, S.; Kohlbacher, O.; Ottmann, C. Virtual screening and experimental validation reveal novel small-molecule inhibitors of 14-3-3 protein–protein interactions. *Chem. Commun.*. **2013**, *49*, 8468–8470.

(28) Wijffels, G.; Johnson, W. M.; Oakley, A. J.; Turner, K.; Epa, V. C.; Briscoe, S. J.; Polley, M.; Liepa, A. J.; Hofmann, A.; Buchardt, J.; Christensen, C.; Prosselkov, P.; Dalrymple, B. P.; Alewood, P. F.; Jennings, P. A.; Dixon, N. E.; Winkler, D. A. Binding inhibitors of the bacterial sliding clamp by design. *J. Med. Chem.* **2011**, *54*, 4831–4838.

(29) Wijffels, G.; Dalrymple, B. P.; Prosselkov, P.; Kongsuwan, K.; Epa, V. C.; Lilley, P. E.; Jergic, S.; Buchardt, J.; Brown, S. E.; Alewood, P. F.; Jennings, P. A.; Dixon, N. E. Inhibition of protein interactions with the β_2 sliding clamp of *Escherichia coli* DNA polymerase III by peptides derived from β_2-binding proteins. *Biochemistry.* **2004**, *43*, 5661–5671.

(30) Yin, Z.; Kelso, M. J.; Beck, J. L.; Oakley, A. J. Structural and thermodynamic dissection of linear motif recognition by the *E. coli* sliding clamp. *J. Med. Chem.* **2013**, *56*, 8665–8673.

(31) Kongsuwan, K.; Josh, P.; Picault, M. J.; Wijffels, G.; Dalrymple, B. The plasmid RK2 replication initiator protein (TrfA) binds to the sliding clamp β subunit of DNA polymerase III: implication for the toxicity of a peptide derived from the amino-terminal portion of 33-kilodalton TrfA. *J. Bacteriol.* **2006**, *188*, 5501–5509.

(32) Dohrmann, P. R.; McHenry, C. S. A bipartite polymerase-processivity factor interaction: only the internal β binding site of the α subunit is required for processive replication by the DNA polymerase III holoenzyme. *J. Mol. Biol.* **2005**, *350*, 228–239.

(33) Wolff, P.; Olieric, V.; Briand, J. P.; Chaloin, O.; Dejaegere, A.; Dumas, P.; Ennifar, E.; Guichard, G.; Wagner, J.; Burnouf, D. Y. Structure-based design of short peptide ligands binding onto the *E. coli* processivity ring. *J. Med. Chem.* **2011**, *54*, 4627–4637.

(34) Kenakin, T. Radioligand binding experiments. In *Pharmacologic Analysis of Drug-Receptor Interaction*, 2nd ed.; Raven Press, 1993; pp. 385-410.

(35) Irwin, J. J.; Sterling, T.; Mysinger, M. M.; Bolstad, E. S.; Coleman, R. G. ZINC: a free tool to discover chemistry for biology. *J. Chem. Inf. Model.* **2012**, *52*, 1757–1768.

(36) Lang, P. T.; Moustakas, D.; Brozell, S.; Carrascal, N.; Mukherjee, S.; Pegg, S.; Raha, K.; Shivakumar, D.; Rizzo, R.; Case, D.; Shoichet, B.; Kuntz., I. *DOCK, Version 6.2*; University of California, San Francisco, USA, 2008.

(37) Mortenson, P. N.; Murray, C. W. Assessing the lipophilicity of fragments and early hits. *J. Comput. Aided Mol. Des.* **2011**, *25*, 663–667.

(38) Oakley, A. J.; Prosselkov, P.; Wijffels, G.; Beck, J. L.; Wilce, M. C.; Dixon, N. E. Flexibility revealed by the 1.85-Å crystal structure of the β sliding-clamp subunit of *Escherichia coli* DNA polymerase III. *Acta Crystallogr. D Biol. Crystallogr.* **2003**, *59*, 1192–1199.

(39) Jergic, S.; Horan, N. P.; Elshenawy, M. M.; Mason, C. E.; Urathamakul, T.; Ozawa, K.; Robinson, A.; Goudsmits, J. M.; Wang, Y.; Pan, X.; Beck, J. L.; van Oijen, A. M.; Huber, T.; Hamdan, S. M.; Dixon, N. E. A direct proofreader–clamp interaction stabilizes the Pol III replicase in the polymerization mode. *EMBO J.* **2013**, *32*, 1322–1333.

(40) Naktinis, V.; Onrust, R.; Fang, L.; O'Donnell, M. Assembly of a chromosomal replication machine: two DNA polymerases, a clamp loader, and sliding clamps in one holoenzyme particle. II. Intermediate complex between the clamp loader and its clamp. *J. Biol. Chem.* **1995**, *270*, 13358–13365.

(41) Leu, F. P.; O'Donnell, M. Interplay of clamp loader subunits in opening the β sliding clamp of *Escherichia coli* DNA polymerase III holoenzyme. *J. Biol. Chem.* **2001**, *276*, 47185–47194.

(42) Jeruzalmi, D.; Yurieva, O.; Zhao, Y.; Young, M.; Stewart, J.; Hingorani, M.; O'Donnell, M.; Kuriyan, J. Mechanism of processivity clamp opening by the δ subunit wrench of the clamp loader complex of *E. coli* DNA polymerase III. *Cell* **2001**, *106*, 417–428.

(43) Beck, J. L.; Urathamakul, T.; Watt, S. J.; Sheil, M. M.; Schaeffer, P. M.; Dixon, N. E. Proteomic dissection of DNA polymerization. *Expert Rev. Proteomics* **2006**, *3*, 197–211.

(44) Kelch, B. A.; Makino, D. L.; O'Donnell, M.; Kuriyan, J. How a DNA polymerase clamp loader opens a sliding clamp. *Science* **2011**, *334*, 1675–1680.

(45) Chilingaryan, Z.; Yin, Z.; Oakley, A. J. Fragment-based screening by protein crystallography: successes and pitfalls. *Int. J. Mol. Sci.* **2012**, *13*, 12857–12879.

(46) Wilson, C. G.; Arkin, M. R. Probing structural adaptivity at PPI interfaces with small molecules. *Drug Discov. Today Technol.* **2013**, *10*, e501–e508.

(47) Rees, D. C.; Congreve, M.; Murray, C. W.; Carr, R. Fragment-based lead discovery. *Nat. Rev. Drug Discov.* **2004**, *3*, 660–672.

(48) Mason, C. E.; Jergic, S.; Lo, A. T.; Wang, Y.; Dixon, N. E.; Beck, J. L. *Escherichia coli* single-stranded DNA-binding protein: A nanoESI-MS study of salt-modulated subunit exchange and DNA binding transactions. *J. Am. Soc. Mass Spectrom.* **2013**, *24*, 274–285.

(49) McPhillips, T. M.; McPhillips, S. E.; Chiu, H. J.; Cohen, A. E.; Deacon, A. M.; Ellis, P. J.; Garman, E.; Gonzalez, A.; Sauter, N. K.; Phizackerley, R. P.; Soltis, S. M.; Kuhn, P. Blu-Ice and the Distributed Control System: software for data acquisition and instrument control at macromolecular crystallography beamlines. *J. Synchrotron Radiat.* **2002**, *9*, 401–406.

(50) Otwinowski, Z.; Minor, W. Processing of X-ray diffraction data collected in oscillation mode. *Methods Enzymol.* **1997**, 276, 307–326.

(51) Winn, M. D.; Ballard, C. C.; Cowtan, K. D.; Dodson, E. J.; Emsley, P.; Evans, P. R.; Keegan, R. M.; Krissinel, E. B.; Leslie, A. G.; McCoy, A.; McNicholas, S. J.; Murshudov, G. N.; Pannu, N. S.; Potterton, E. A.; Powell, H. R.; Read, R. J.; Vagin, A.; Wilson, K. S. Overview of the CCP4 suite and current developments. *Acta Crystallogr. D Biol. Crystallogr.* **2011**, *67*, 235–242.

(52) Emsley, P.; Cowtan, K. Coot: model-building tools for molecular graphics. *Acta Crystallogr. D Biol. Crystallogr.* **2004**, *60*, 2126–2132.

(53) Skubak, P.; Murshudov, G. N.; Pannu, N. S. Direct incorporation of experimental phase information in model refinement. *Acta Crystallogr. D Biol. Crystallogr.* **2004**, *60*, 2196–2201.

(54) CLSI. Methods for dilution antimicrobial susceptibility tests for bacteria that grow aerobically; approved standard; CLSI: Wayne, PA., **2009**.

Table of Contents artwork

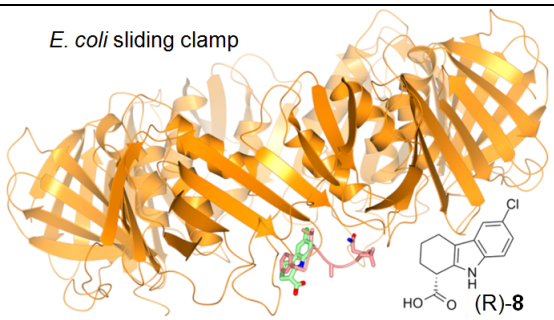

Discovery of Lead Antibacterials Targeting the *E. coli* Sliding Clamp using a Fragment-Based Approach

Zhou Yin,[†] Louise R. Whittell,[†] Yao Wang,[†] Slobodan Jergic,[†] Michael Liu,[‡] Elizabeth J. Harry,[‡] Nicholas E. Dixon,[†] Jennifer L. Beck,[†] Michael J. Kelso,[†] and Aaron J. Oakley[†]*

[†]School of Chemistry and Centre for Medical and Molecular Bioscience, University of Wollongong, New South Wales, Australia.

[‡]ithree Centre, University of Technology, Sydney, New South Wales, Australia

*e-mail: aarono@uow.edu.au

SUPPORTING INFORMATION

Supplementary Data

Table S1. Data collection and refinement statistics for X-ray co-crystal structures of the *E. coli* SC in complex with fragment hits **1**–**4** (i.e. complexes SC^1 – SC^4, respectively).

Name	**SC^1**	**SC^2**	**SC^3**	**SC^4**
PDB Code	4N94	4N95	4N96	4N97
Data collection				
Space group	P1	P1	P1	P1
Cell dimensions	a, b, c (Å) / α, β, γ (°) 40.74, 64.51, 71.72 / 74.01, 83.21, 84.54	a, b, c (Å) / α, β, γ (°) 40.99, 65.51, 73.44/ 73.03, 85.29, 85.65	a, b, c (Å) / α, β, γ (°) 40.88, 64.67, 72.02 / 73.97, 83.55, 84.36	a, b, c (Å) / α, β, γ (°) 40.88, 64.78, 72.59 / 73.91, 84.51, 84.89
Resolution (Å)	30.38–1.73(1.82–1.73)	28.86–1.80 (1.90–1.80)	30.51–1.70 (1.79–1.70)	28.9–1.97 (2.08–1.97)
R_{merge} (%)	6.7 (55.1)	6.4 (39.9)	4.8 (32.8)	5.6 (19.1)
No. of Reflections	242483	235693	242187	153662
Unique	66608 (8933)	61187 (8833)	64167 (9074)	42650 (6264)
Mean I/σ(I)	9.9 (2.1)	14.3 (3.2)	15.2 (3.4)	12.7 (6.4)
Completeness (%)	91.7 (84.2)	95.9 (94.7)	83.0 (80.4)	84.8 (85.2)
Multiplicity	3.6 (3.6)	3.9 (3.8)	3.8 (3.7)	3.6 (3.3)
Refinement				
Resolution (Å)	28.91–1.73 (1.78–1.73)	28.32–1.80 (1.85–1.80)	28.72–1.70 (1.74–1.70)	28.9–1.97 (2.02–1.97)
R_{work}/R_{free} (%)	25.1 (35.5)/29.2 (44)	18.6 (26.4)/22.4 (30.3)	22.7 (33.2)/27.5 (42.0)	23.2 (30.9)/30.6 (42.7)
R.m.s deviations				
Bond lengths (Å)	0.0098	0.0068	0.0083	0.0077
Bond angles (°)	1.4687	1.2819	1.3235	1.3011
B-factors				
M. Chain	20.6	18.5	19.3	20.25
S. Chain & Water	24.2	23.3	22.6	22.89
Ligands*	41.5	49.7	26.6	35.1
Ramachandran Plot Outliers	0.57%	0.44 %	0.58 %	0.58 %

Values for data in the highest resolution shell are given in parentheses.

Diffraction data were collected at Beamline MX1, Australian Synchrotron, at a wavelength of 0.95 Å. Diffraction data were processed with MOSFLM and SCALA.

*Ligands refer to the fragment compounds bound to Chain A.

Table S2. Data collection and refinement statistics for X-ray co-crystal structures of the *E. coli* SC in complex with compounds **5**, **7** and (*R*)-**8** (i.e. complexes SC^5 – SC^7 and SC^8, respectively).

Name	**SC^5**	**SC^7**	**SC^8**
PDB Code	4N98	4N99	4N9A
Data collection			
Space group	$P2_1$	P1	$P2_1$
Cell dimensions	a, b, c (Å) / α, β, γ (°) 79.90, 67.16, 81.06 / 90.00, 114.11, 90.00	a, b, c (Å) / α, β, γ (°) 41.01, 65.13, 73.24 / 72.95, 85.06, 85.24	a, b, c (Å) / α, β, γ (°) 79.78, 67.37, 81.12 / 90.00, 113.92, 90.00
Resolution (Å)	30.50–1.70 (1.79–1.70)	40.95–2.30 (2.42–2.30)	43.86–1.90 (2.00–1.90)
R_{merge} (%)	9.7 (68.3)	14.7 (64.3)	5.2(39.7)
No. of Reflections	603665	112766	137425
Unique Reflections	86092 (12490)	29744 (4227)	57937 (7647)
Mean I/σ(I)	9.2 (2.4)	8.5 (2.2)	9.8 (2.4)
Completeness (%)	99.9 (99.8)	92.9 (89.9)	93.7 (85.6)
Multiplicity	7.0 (6.9)	3.8 (3.7)	2.4 (2.3)
Refinement			
Resolution (Å)	30.17–1.70 (1.74–1.70)	40.95–2.30 (2.36–2.30)	36.46–1.90 (1.95–1.90)
R_{work}/R_{free} (%)	25.6 (30.0)/29.6 (35.5)	26.1 (32.1)/33.7 (42.9)	21.4 (38.8)/26.1(40.7)
R.m.s. deviations			
Bond lengths (Å)	0.0079	0.0042	0.0090
Bond angles (°)	1.2817	0.8770	1.3791
B-factors			
M. Chain	22.3	21.0	28.1
S. Chain & Water	26.4	23.1	33.2
Ligands*	39.8	51.7	42.1
Ramachandran Plot Outliers	0.58%	0.56 %	0.72 %

Values for data in the highest resolution shell are given in parentheses.

Diffraction data for SC^5 were collected at Beamline MX1, Australian Synchrotron, at a wavelength of 0.95 Å.

Diffraction data for SC^7 and SC^8 were collected using an in-house X-ray generator (University of Wollongong) at a wavelength of 1.5418 Å.

Diffraction data were processed with MOSFLM and SCALA.

*Ligands refer to the compounds bound to Chain A.

Table S3: Binding data for carbazole and tetrahydrocarbazole derivatives against the *E. coli* SC.

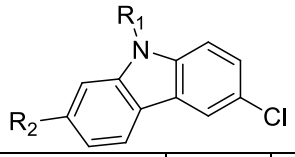

cpd	R_1	R_2	IC_{50} (μM)	K_i (μM)	LE (kcal/ mol)	LogD (pH 7.2)	LLE_{AT}
6a	H	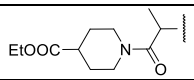	> 1000	n/a	n/a	n/a	n/a
6b	H	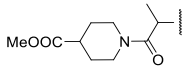	885	492	0.16	4.41	0.06
6c	H	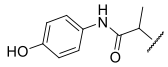	> 1000	n/a	n/a	n/a	n/a

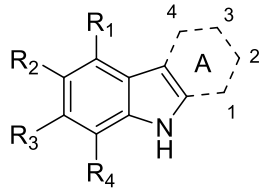

cpd	R_1	R_2	R_3	R_4	ring A	IC_{50} (μM)	K_i (μM)	LE (kcal/ mol)	LogD (pH 7.2)	LLE_{AT}
11	H	H	H	Cl	3-CO_2Me cyclohexyl	851	473	0.25	3.91	0.07
12	H	Cl	CO_2H	H	cycloheptyl	877	487	0.25	–0.16	0.38
13	H	CO_2H	Cl	H	cyclohexyl	> 1000	n/a	n/a	n/a	n/a
14	Cl	CO_2H	H	H	cyclohexyl	> 1000	n/a	n/a	n/a	n/a
15	H	Cl	H	H	3-CO_2Et cyclohexyl	> 1000	n/a	n/a	n/a	n/a
16	H	Cl	H	H	3-CO_2H cyclohexyl	> 1000	n/a	n/a	n/a	n/a
17	H	Cl	H	H	3-CO_2Me cyclohexyl	> 1000	n/a	n/a	n/a	n/a
18	H	Cl	H	H	cyclopentyl	> 1000	n/a	n/a	n/a	n/a
19	H	Cl	H	H	3-piperidinyl	> 1000	n/a	n/a	n/a	n/a
20	H	Cl	H	H	cycloheptyl	> 1000	n/a	n/a	n/a	n/a
21	Cl	H	H	H	1-CO_2Me cyclohexyl	> 1000	n/a	n/a	n/a	n/a
22	H	H	H	Cl	cyclohexyl	> 1000	n/a	n/a	n/a	n/a
23	H	H	H	Cl	3-CO_2Et cyclohexyl	> 1000	n/a	n/a	n/a	n/a
24	H	H	H	Cl	3-CO_2H cyclohexyl	> 1000	n/a	n/a	n/a	n/a
25	H	Cl	OH	H	cyclohexyl	> 1000	n/a	n/a	n/a	n/a
26	CO_2H	Cl	H	H	2-CO_2H cyclohexyl	> 1000	n/a	n/a	n/a	n/a
27	CO_2H	Cl	H	H	cyclopentyl	> 1000	n/a	n/a	n/a	n/a
28	CO_2H	Cl	H	H	cycloheptly	> 1000	n/a	n/a	n/a	n/a
29	H	Cl	CO_2Me	H	cyclohexyl	> 1000	n/a	n/a	n/a	n/a

n/a: not applicable

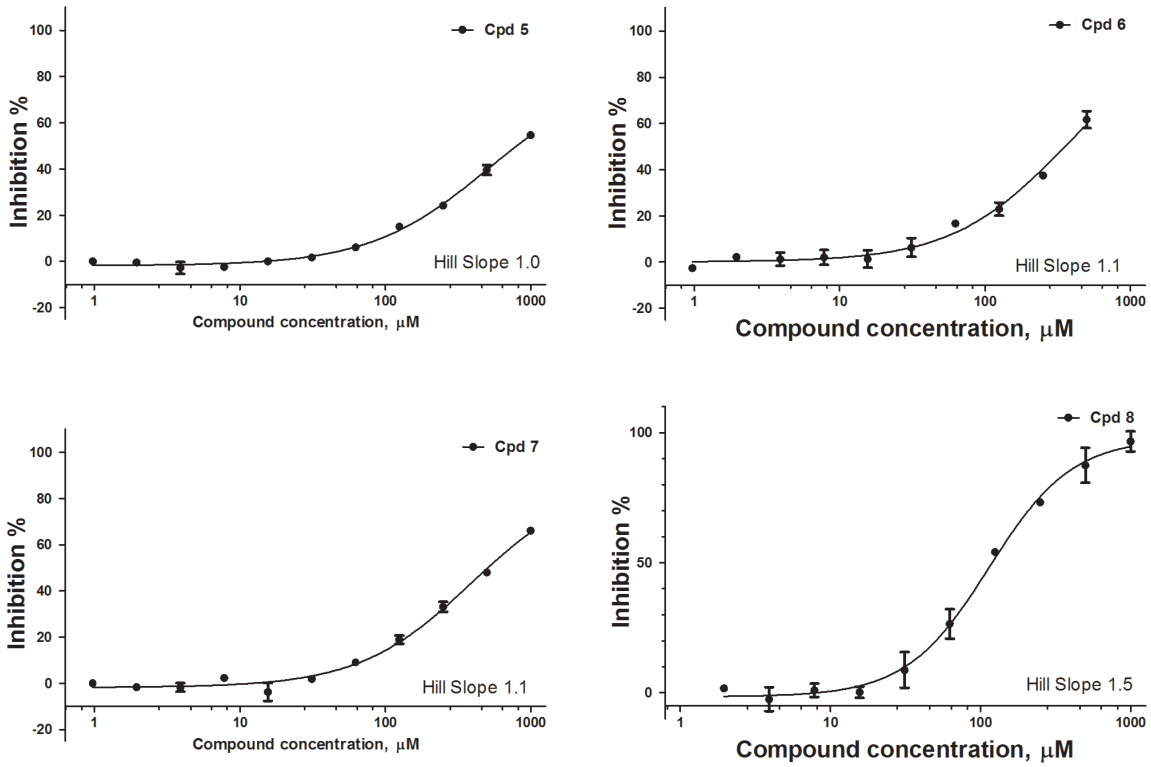

Figure S1. Inhibition of binding of a fluorescently labelled tracer peptide (5FAM-QLDLF) to the *E. coli* SC. Data are standardized and shown as inhibition (%, decreased polarization divided by background subtracted total polarization). Error bars represent standard deviation (n=2).

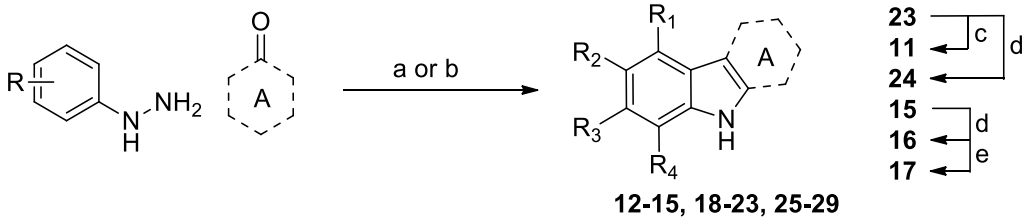

Scheme S1. Synthesis of substituted tetrahydrocarbazoles **11**–**29**. Reagents: (a) AcOH or EtOH and HCl (cat)), ketone, reflux, 3–64%; (b) i) AcOH, ketone, reflux, ii) MeOH, H_2SO_4 (cat.) reflux, 18%; (c) i) NaOH, EtOH, rt., ii) MeOH, H_2SO_4 (cat.) reflux, 44%; (d) NaOH, EtOH, rt, 31–47%; (e) MeOH, H_2SO_4 (cat.) reflux, 65%.

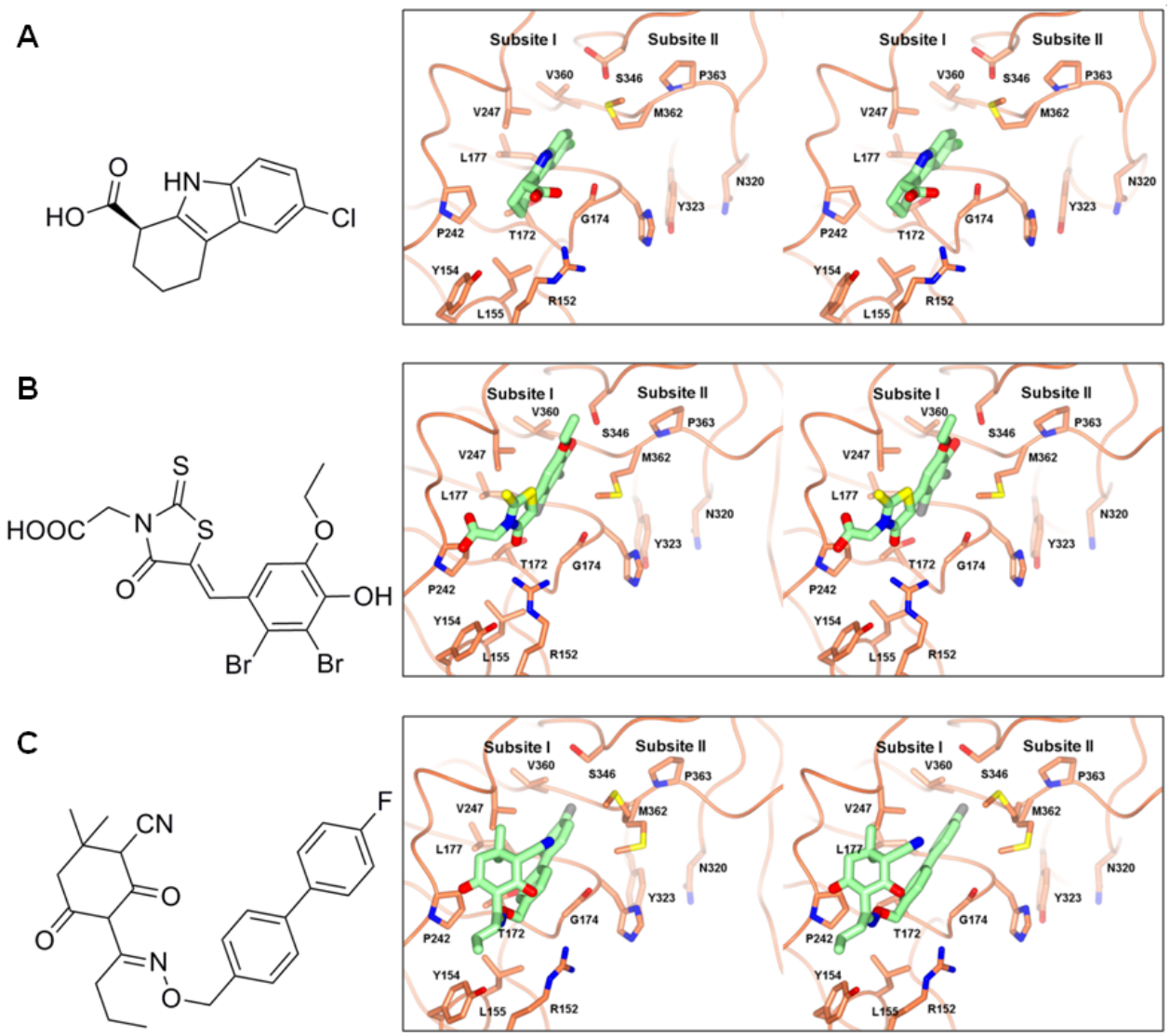

Figure S2. Stereo diagrams of (**A**) (*R*)-**8**, (**B**) RU7 reported by Georgescu *et al.*[1] and (**C**) a biphenyloxime ether derivative reported by Wijffels *et al.*[2] binding to subsite I of the *E. coli* SC LM-binding pocket. Carbon atoms of the inhibitors are colored light green and the SC carbon atoms are colored orange. Other atoms are in CPK colors.

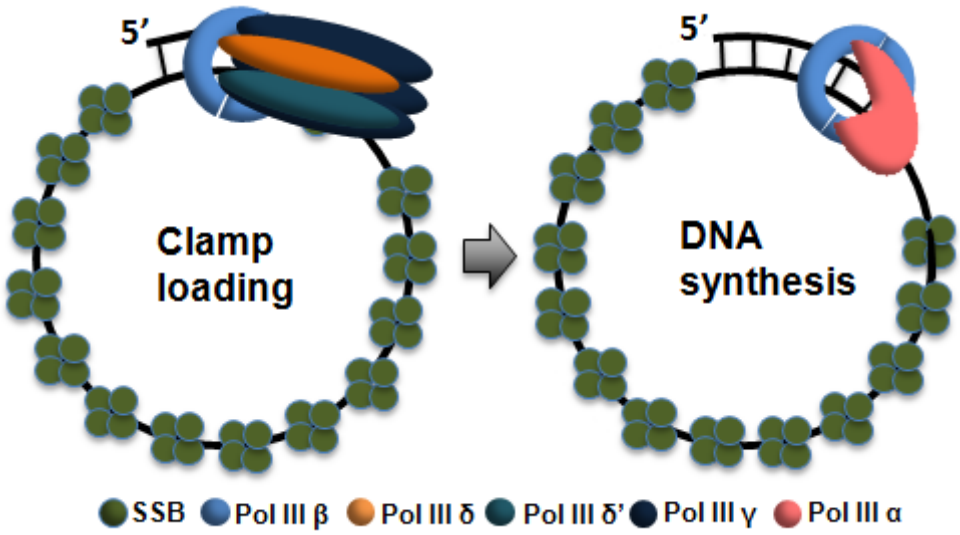

Figure S3. Schematic representation of the *in vitro* DNA replication assay.

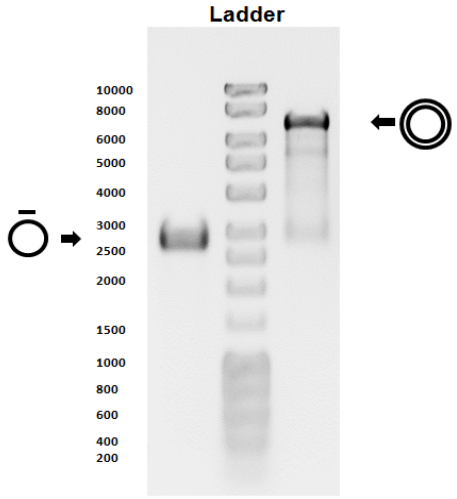

Figure S4. *In vitro* DNA replication control assay carried out in the presence of 3.5% DMSO (no inhibitor). Molecular sizes (in bp for dsDNA) corresponding to bands in the DNA ladder are shown. Circles with a dash represent primed ssDNA template. Concentric circles represent dsDNA replication products.

Table S4: Optical density (absorbance at 595 nM) measured for 24h bacterial growth under varying compound concentrations.*

E. coli	**Compound concentration (μM)**											
Compd.	**5000**	**2500**	**1250**	**625**	**312.5**	**156.25**	**78.13**	**39.06**	**19.53**	**9.77**	**4.88**	**2.44**
5	-0.11	0.05	0.12	0.15	0.20	0.13	0.20	0.17	0.13	0.15	0.14	0.14
7	0.01	0.07	0.20	0.17	0.18	0.16	0.14	0.11	0.14	0.14	0.12	0.17
8	-0.57	-0.29	-0.08	-0.04	-0.01	0.16	0.15	0.24	0.12	0.14	0.15	0.18
9	-0.02	-0.03	-0.08	-0.06	-0.04	-0.02	0.16	0.15	0.15	0.13	0.12	0.17
10	-0.35	-0.15	-0.14	-0.11	-0.09	0.02	0.03	0.13	0.12	0.15	0.15	0.17
A. baylyi	**Compound concentration (μM)**											
Compd.	**5000**	**2500**	**1250**	**625**	**312.5**	**156.25**	**78.13**	**39.06**	**19.53**	**9.77**	**4.88**	**2.44**
5	-0.20	0.31	0.42	0.44	0.49	0.39	0.39	0.38	0.46	0.45	0.46	0.39
7	0.01	0.19	0.37	0.46	0.52	0.48	0.53	0.46	0.38	0.47	0.45	0.49
8	-0.57	-0.28	-0.10	-0.03	0.07	0.34	0.39	0.39	0.38	0.39	0.48	0.45
9	-0.07	-0.04	-0.01	0.07	0.03	0.04	0.04	0.39	0.40	0.41	0.41	0.45
10	-0.28	-0.09	-0.09	0.01	0.01	0.03	0.37	0.39	0.39	0.43	0.39	0.45
B. subtilis	**Compound concentration (μM)**											
Compd.	**5000**	**2500**	**1250**	**625**	**312.5**	**156.25**	**78.13**	**39.06**	**19.53**	**9.77**	**4.88**	**2.44**
5	-0.08	0.01	0.15	0.21	0.21	0.23	0.18	0.18	0.16	0.15	0.19	0.27
7	0.00	0.08	0.11	0.13	0.16	0.20	0.23	0.24	0.24	0.24	0.22	0.21
8	-0.33	-0.17	-0.04	-0.02	0.00	0.00	0.13	0.19	0.26	0.23	0.23	0.23
9	0.01	-0.01	-0.05	-0.05	-0.03	-0.01	0.08	0.20	0.22	0.22	0.20	0.23
10	-0.33	-0.10	-0.03	-0.04	-0.06	-0.04	0.07	0.15	0.18	0.19	0.22	0.21
S. aureus	**Compound concentration (μM)**											
Compd.	**5000**	**2500**	**1250**	**625**	**312.5**	**156.25**	**78.13**	**39.06**	**19.53**	**9.77**	**4.88**	**2.44**
5	-0.09	0.13	0.20	0.17	0.18	0.19	0.19	0.22	0.21	0.17	0.22	0.23
7	0.00	0.07	0.12	0.16	0.19	0.15	0.18	0.17	0.18	0.14	0.17	0.21
8	-0.35	-0.17	-0.01	-0.02	0.00	0.00	0.10	0.15	0.17	0.22	0.18	0.21
9	0.00	-0.01	-0.05	-0.05	-0.03	0.05	0.18	0.21	0.27	0.23	0.21	0.23
10	-0.32	-0.09	-0.02	-0.04	-0.06	-0.04	0.04	0.19	0.17	0.22	0.23	0.22

*Optical density values are subtracted of the background.

Supplementary Methods

Molecular Docking and Chemo-Informatics. Fragment scaffolds were used for similarity and/ or substructure searches in the UCSF ZINC library.[3] A number of larger scaffolds were used for substructure search of commercially available compounds for molecular docking using UCSF DOCK 6.5.[4] The receptor was prepared by removing all crystallographic water molecules from the sidling clamp except for a structurally conserved water molecule near residue M362. Residues greater than 15 Å away from the binding pocket were deleted. Hydrogen atoms were added and partial charges were assigned. Ligands were prepared using UCSF Chimera or downloaded from UCSF ZINC library. Spheres for ligand orientations were generated using the identified fragment binders. A grid map for scoring was generated encompassing residues within 15 Å of the spheres. Docking was carried out using Grid score as the primary score and GB/SA Hawkins score as a secondary scoring method. The top 50 poses were clustered and the top 10 cluster heads assessed using the secondary scoring method. Additionally, Amber scoring[5] was performed with 100 steps of minimization, 3000 md cycles and another 100 minimization steps, each step corresponded to 2 fs. In all cases ligand flexibility was allowed and the receptor kept rigid. Selected molecules were acquired for testing.

Calculation of *Log*D values at pH 7.2 was performed using Accord for Excel 6.2 (Accelrys).

The equations used to determine LE and LLE_{AT} followed the published methods[6] and are detailed below:

$$LE = -\Delta G/HAC$$

$$= -RTln(K_i)/HAC$$

$$\Delta G^* = \Delta G - \Delta G_{lipo}$$

$$= RTln(K_i) + RTLogD$$

$$LLE_{AT} = 0.11 - \Delta G^*/HAC$$

LE: ligand efficiency; ΔG: delta Gibbs energy; K_i: inhibition constant; HAC: heavy atom count; *log*D: distribution coefficient at pH 7.2; LLE_{AT}: ligand lipophilicity efficiency.

Organic Synthesis. ^1H and ^{13}C NMR spectra were acquired on a Varian Mercury 300 MHz, Varian Inova 500 MHz or VNMRS 500 MHz spectrometer. Chemical shifts (δ) are reported in ppm relative to the solvent and coupling constants (J) are given in Hz. Electrospray (EI) LRMS were recorded on a Waters Micromass Platform LCZ spectrometer and HRMS were recorded on a Waters Xevo spectrometer, using an EI or ASAP source. Melting points were recorded using a Gallenkamp (Griffin) melting point apparatus and are uncorrected. Optical rotations for chiral compounds were measured on a Jasco P-2000 polarimeter. TLC was performed on precoated Merck silica gel 60 PF_{254} aluminium sheets and flash column chromatography (FCC) performed with Davisil silica gel (40–63 μm). Petrol refers to petroleum spirits of bp 40–60°C. 2-chloro-4-hydrazinobenzoic acid hydrochloride (**31**) and 2-chloro-5-hydrazinobenzoic acid hydrochloride (**32**) were prepared as previoulsy reported by Green *et al.*[7] (see general hydrazine formation procedure) from 2-chloro-4-aminobenzoic acid and 2-chloro-5-amino-benzoic acid respectively. All final compounds have a purity of ≥ 95% by proton NMR.

General Fischer Indole Procedure. To a solution of the phenylhydrazine in glacial acetic acid (or absolute ethanol with HCl (cat.)) was added the ketone, and the resulting mixture refluxed for 2–17 h. The reaction mixture was cooled, concentrated and extracted with EtOAc (or CH_2Cl_2). The combined extracts were washed with water, brine, dried ($MgSO_4$), concentrated and the residue purified by either recrystallisation or FCC.

General Esterification Procedure. To a solution of the carboxylic acid in methanol (or ethanol), concentrated H_2SO_4 (cat.) was added and the solution refluxed for 2–23 h. The mixture was cooled, concentrated, neutralised with saturated $NaHCO_3$ (aq) solution and extracted with CH_2Cl_2. The combined extracts were washed with brine, dried ($MgSO_4$), concentrated and the residue purified by recrystallisation or trituration.

General Deesterification Procedure. To a solution of the ester in absolute ethanol, sodium hydroxide (2 M) was added and the reaction mixture stirred at room temperature for 2–17 h. The reaction mixture was concentrated, diluted with water and washed with CH_2Cl_2. The aqueous layer was subsequently acidified with 1 M HCl and extracted with CH_2Cl_2. The combined extracts were washed with brine, dried ($MgSO_4$) and concentrated. The residue was either used crude in subsequent reactions or purified by recrystallisation or trituration.

General Hydrazine Formation Procedure. A suspension of the amine in concentrated HCl was stirred for 30 min in an ice/salt bath and then a cooled solution of $NaNO_2$ in water added drop wise. The solution was stirred for 1 h and a cooled solution of $SnCl.2H_2O$ in concentrated HCl added drop wise. The suspension was allowed to warm to room temperature overnight and the resulting precipitate collected by vacuum filtration (washing with cold water then Et_2O).

Methyl 8-chloro-2,3,4,9-tetrahydro-1H-carbazole-3-carboxylate (11)

General Fischer indole procedure with 2-chlorophenylhydrazine hydrochloride (310.3 mg, 1.73 mmol) and ethyl-4-oxocyclohexane-1-carboxylate (268.1 mg, 1.58 mmol) provided ethyl 8-chloro-2,3,4,9-tetrahydro-1H-carbazole-3-carboxylate (**23;** 240.5 mg, 0.87 mmol, 55% yield) as a pale yellow crystalline solid following recrystallisation from methanol, mp 152 – 154 °C. ^{1}H NMR ($CDCl_3$, 500 MHz): 1.29 (3H, t, *J* = 7.5 Hz), 2.00-2.07 (1H, m), 2.30-2.32 (1H, m), 2.76-2.92 (4H, m), 3.00 (1H, dd, *J* = 15.5 , 4.8 Hz), 4.20 (2H, q, *J* = 6.7 Hz), 7.00 (1H, t, *J* = 8.0 Hz), 7.11 (1H, d, *J* = 8.0 Hz), 7.35 (1H, d, *J* = 7.5 Hz), 7.98 (1H, s). ^{13}C NMR ($CDCl_3$, 125MHz): 14.4, 22.4, 24.1, 25.8, 40.4, 60.6, 110.0, 116.1, 116.5, 120.2, 120.9, 129.2, 133.4, 134.0, 175.3. LRMS (ES^+) *m/z*: 316.23 $[M+K]^+$. HRMS (ES^+) calcd. for $C_{15}H_{17}NO_2Cl$ $[M+H]^+$ 278.0948, found. 278.0948.

General deesterification procedure with **23** (109.9 mg, 0.40 mmol), followed by general esterification procedure on the crude product in methanol provided **11** (46.0 mg, 44% yield) as an off-white crystalline solid following recrystallisation from methanol, mp 164 - 166°C. ^{1}H NMR ($CDCl_3$, 500 MHz): 2.01-2.08 (1H, m), 2.30-2.33 (1H, m), 2.80-2.93 (4H, m), 3.06-3.07 (1H, m), 3.74 (3H, s), 7.00 (1H, t, *J* = 7.8 Hz), 7.12 (1H, d, *J* = 7.5 Hz), 7.35 (1H, d, *J* = 7.5 Hz), 7.84 (1H, br s). ^{13}C NMR ($CDCl_3$, 125 MHz): 22.4, 24.0, 25.7, 40.2, 52.0, 109.8, 116.1, 116.5, 120.3, 120.9, 129.1, 133.3, 134.0, 175.9. LRMS (ES^-) *m/z*: 261.75 $[M-H]^-$. HRMS (ES^-) calcd. for $C_{14}H_{13}NO_2Cl$ $[M-H]^-$ 262.0635, found 262.0627.

9-chloro-1,2,3,4,5,6-hexahydrocyclohepta[b]indole-8-carboxylic acid (12) and 9-chloro-1,2,3,4,5,6-hexahydrocyclohepta[b]indole-10-carboxylic acid (28)

General Fischer indole procedure with 2-chloro-5-hydrazinobenzoic acid hydrochloride (**32**; 487.1 mg, 2.18 mmol) and cycloheptanone (206.7 mg, 1.84 mmol) in glacial acetic acid (4 mL) produced a mixture of two isomers. The two products were obtained following FCC on silica gel (gradient elution; 30:70:0.5-70:30:0.5 Et_2O/petrol/acetic acid) and recrystallisation of each isomer from methanol/water. **12** (32.0 mg, 7% yield) was obtained as a beige powder, mp >250 °C (dec.). ^{1}H NMR (d_6-DMSO, 300 MHz): 1.65-1.70 (4H, m,), 1.84 (2H, m), 2.70-2.74 (2H, m), 2.82-2.86 (2H, m), 7.48 (1H, s,), 7.79 (1H, s), 11.21 (1H, s), 12.78 (1H, s). ^{13}C NMR (d_6-DMSO, 75 MHz): 24.1, 26.9, 28.4, 28.7, 31.4, 112.6, 114.3, 18.7, 120.4, 122.2, 131.6, 131.8, 143.9, 167.3. LRMS (ES^-) *m/z*: 262.0 $[M-H]^-$. HRMS ($ASAP^-$) calcd. for $C_{14}H_{13}NO_2Cl$ $[M-H]^-$262.0635, found 262.0626. **28** (12.3 mg, 3% yield) was obtained as a red/brown powder, mp 118 -120 °C. ^{1}H NMR (d_6-DMSO, 500 MHz): 1.61-1.68 (2H, m), 1.67-1.68 (2H, m), 1.79-1.80 (2H, m), 2.66 (2H, t like, *J* = 5.25 Hz), 2.80 (2H, *t* like, *J* = 5.5 Hz), 6.97 (1H, d, *J* = 8.5 Hz), 7.25 (1H, d, *J* = 8.5 Hz), 11.12 (1H, s), 13.25 (1H, br s). ^{13}C NMR (d_6-DMSO, 75 MHz): 24.2, 26.7, 28.1, 28.2, 31.2, 111.5, 112.4, 118.6, 119.6, 124.7, 124.8, 133.0, 141.6, 168.9. LRMS (ES^-) *m/z*: 262.0 $[M-H]^-$. HRMS (ES^-) calcd. for $C_{14}H_{13}NO_2Cl$ $[M-H]^-$ 262.0635, found 262.0642.

7-chloro-2,3,4,9-tetrahydrocarbazole-6-carboxylic acid (13) and 5-chloro-2,3,4,9-tetrahydrocarbazole-6-carboxylic acid (14)[8]

General Fischer indole procedure with 2-chloro-4-hydrazinobenzoic acid hydrochloride (**31**; 549.8 mg, 2.46 mmol) and cyclohexanone (300.6 mg, 3.06 mmol) in glacial acetic acid (3 mL) produced a mixture of two isomers. The two products were obtained following FCC on silica gel (gradient elution; 2:8–6:46 Et_2O/petrol) and recrystallisation of each isomer from methanol/water. **13** (16.9 mg, 3% yield) was obtained as a beige powder, mp 248 – 250 °C. ^{1}H NMR (MeOD, 500 MHz): 1.87-1.92 (4H, m), 2.68 (2H, d, *J* = 5 Hz), 2.72 (2H, d, *J*= 5.5 Hz), 7.31 (1H, s), 7.97 (1H, s). ^{13}C NMR ($CDCl_3$+d_6-DMSO, 125 MHz): 20.4, 22.6, 22.7, 22.9, 110.3, 112.4, 119.5, 122.0, 125.6, 125.8, 136.5, 137.6, 168.5 (CO_2H). LRMS (ES^+) *m/z*: 272.2 $[M+23]^+$. HRMS ($ASAP^+$) calcd. for $C_{13}H_{13}NO_2Cl$ $[M+H]^+$ 250.0635, found 250.0699. **14** (19.9mg, 3% yield) was obtained as a pink powder, mp 242 -244 °C. ^{1}H NMR ($CDCl_3$+d_6-DMSO, 500 MHz): 1.86 (4H, br s), 2.72 (2H, s), 3.11 (2H, s), 7.15 (1H, d, *J* = 8.5 Hz), 7.63 (1H, d, *J* = 8.5 Hz), 9.78 (1H, br s). ^{13}C NMR ($CDCl_3$+d_6-DMSO, 125 MHz): 22.3, 23.3, 23.4, 108.6, 111.1, 120.3, 123.8, 125.9, 136.6, 138.3, 168.7. LRMS (ES^-) *m/z*: 247.9 $[M-H]^-$. HRMS (ES^-) calcd for $C_{13}H_{11}NO_2Cl$ $[M-H]^-$ 248.0478, found. 248.0467.

Ethyl 6-chloro-2,3,4,9-tetrahydro-1H-carbazole-3-carboxylate (15)[9]

General Fischer indole procedure with 4-chlorophenylhydrazine hydrochloride (395.1 mg, 2.21 mmol) and ethyl-4-oxocyclohexane-1-carboxylate (363.3 mg, 2.13 mmol) in absolute ethanol (5.5 mL) provided **15** (378.3 mg, 64% yield) as an off-white crystalline solid following recrystallisation from methanol, mp 134 -136 °C. ^{1}H NMR ($CDCl_3$, 500 MHz): 1.29 (3H, t, *J* = 7Hz), 1.99-2.04 (1H, m), 2.28-2.30 (1H, m), 2.75-2.88 (4H, m), 3.00 (1H, dd, *J* = 15, 5.0 Hz), 4.20 (2H, q, *J* = 7.2 Hz), 7.05 (1H, d, *J* = 8.5 Hz), 7.15 (1H, d, *J* = 8.5 Hz), 7.41 (1H, s), 7.81 (1H, s). ^{13}C NMR ($CDCl_3$, 125MHz): 14.4, 22.4, 23.8, 25.7, 40.3, 60.7, 108.6, 111.5, 117.5,

121.5, 125.1, 128.7, 134.4, 134.8, 175.5. LRMS (ES^+) *m/z*: 316.15 $[M+K]^+$. HRMS (ES^+) calcd. for $C_{15}H_{17}NO_2Cl$ $[M+H]_+$ 278.0948, found 278.0951.

6-chloro-2,3,4,9-tetrahydro-1H-carbazole-3-carboxylic acid (16)

General deesterification procedure with **15** (111.8 mg, 0.40 mmol) provided **16** (47.7 mg, 47% yield) as a beige powder following trituration with CH_2Cl_2, mp 178 -180 °C. ^1H NMR (MeOD, 500 MHz): 1.97-1.99 (1H, m), 2.26-2.29 (1H, m), 2.78-2.82 (4H, m,), 2.96 (1H, d, *J* = 11 Hz), 6.96 (1H, d, *J* = 8 Hz), 7.17 (1H, d, *J* = 8.5 Hz), 7.31 (1H, s), 10.21 (1H, br s). ^{13}C NMR (MeOD, 125 MHz): 23.1, 24.8, 27.0, 41.5, 108.3, 112.5, 117.6, 121.5, 125.2, 129.9, 136.2, 136.6, 179.4 (C). LRMS (ES^-) *m/z*: 247.99 $[M-H]^-$. HRMS (ES^-) calcd. for $C_{13}H_{11}NO_2Cl$ $[M-H]^-$ 248.0478, found 248.0474.

Methyl 6-chloro-2,3,4,9-tetrahydro-1H-carbazole-3-carboxylate (17)

General esterification procedure with **16** (43.7 mg, 0.18 mmol) in methanol provided **17** (30.7 mg, 65% yield) as a pale yellow powder following trituration with petrol, mp 104 - 106 °C. ^1H NMR ($CDCl_3$, 300 MHz): 1.99-2.05 (1H, m), 2.27-2.31 (1H, m), 2.79-3.01 (5H, m), 3.74 (3H, s), 7.05 (1H, dd, *J* = 8.7, 1.5 Hz), 7.14 (1H, d, *J* = 8.4 Hz), 7.40 (1H, s), 7.84 (1H, br s). ^{13}C NMR ($CDCl_3$, 125 MHz): 22.4, 22.8, 25.6, 40.1, 52.0, 108.4, 111.5, 117.5, 121.5, 125.1, 128.7, 134.4, 134.8, 175.9 (C). LRMS (ES^-) *m/z*: 262.04 $[M-H]^-$. HRMS (ES^-) calcd. for $C_{14}H_{13}NO_2Cl$ $[M-H]^-$ 262.0635, found 262.0630.

7-chloro-1,2,3,4-tetrahydrocyclopenta[b]indole (18)[10]

General Fischer indole procedure with 4-chlorophenylhydrazine hydrochloride (429.9 mg, 2.40 mmol) and cyclopentanone (248.4 mg, 2.95 mmol) in glacial acetic acid (4 mL) provided **18** (46.9 mg, 10 % yield) as beige crystalline solid following FCC on silica (gradient elution; 30:70:0.5 - 50:50:0.5 Et_2O/petrol/acetic acid), mp 124 – 126 °C. ^1H NMR (d_6-DMSO, 300 MHz): 2.42-2.47 (2H, m), 2.68-2.73 (2H, m), 2.79-2.84 (2H, m), 6.95 (1H, dd, *J* = 8.4, 2.1 Hz), 7.26 (1H, d, *J* = 8.4 Hz), 7.32 (1H, d, *J* = 2.1 Hz), 11.05 (1H, s). ^{13}C NMR (d_6-DMSO, 125MHz): 23.8, 25.2, 28.1, 112.8, 117.0, 117.4, 119.2, 123.0, 125.1, 139.3, 146.3. LRMS (ES^+) *m/z*: 192.0 $[M+H]^+$. HRMS (ES^+) calcd. for $C_{11}H_{11}NCl$ $[M+H]^+$ 192.0580, found 192.0587.

6-chloro-2,3,4,9-tetrahydro-1H-pyrido[2,1-b]indole hydrochloride (19)[11]

General Fischer indole procedure with 4-piperidinone hydrate hydrochloride (200.8 mg, 1.31 mmol) and 4-chlorophenylhydrazine hydrochloride (244.9 mg, 1.37 mmol) in absolute ethanol (2 mL) provided **19** (43.1 mg, 14% yield) as an off white power following recrystallisation from methanol, mp 278 °C (dec.). ^1H NMR (MeOD, 300 MHz): 3.16-3.18 (2H, br t), 3.59-3.63 (2H,t), 4.40 (2H, s), 7.10 (1H, d, *J* = 8.7 Hz), 7.31 (1H, d, *J* = 8.4 Hz), 7.45 (1H, s). ^{13}C NMR (MeOD, 125MHz): 21.4, 42.1, 42.9, 102.6, 113.4, 117.9, 123.1, 126.3, 127.5, 132.8, 136.3. LRMS (ES^+) *m/z*: 207.09 $[M+H]^+$. HRMS ($ASAP^+$) calcd. for $C_{11}H_{12}N_2Cl$ $[M+H]^+$ 207.0689, found 207.0698.

9-chloro-1,2,3,4,5,6-hexahydrocyclohepta[b]indole (20)[12]

General Fischer indole procedure with 4-chlorophenylhydrazine hydrochloride (442.8 mg, 2.47 mmol) and cycloheptanone (300.9 mg, 2.68 mmol) in glacial acetic acid (4 mL) provided **20** (300.9 mg, 55% yield) as an off-white crystalline solid following recrystallisation from ethanol/water, mp 124 – 126 °C. ^1H NMR (d_6-DMSO, 500 MHz): 1.66-1.68 (4H, m), 1.83 (2H,

m), 2.69-2.70 (2H, m), 2.80-2.81 (2H, m), 6.93 (1H, d, *J* = 8.0 Hz), 7.21 (1H, d, *J* = 8.5Hz), 7.38 (1H, s), 10.87 (1H, br s). ^{13}C NMR (d_6-DMSO, 125MHz): 24.1, 27.0, 28.4, 28.5, 31.4, 111.8, 111.9, 116.3, 119.3, 122.7, 129.8, 132.5, 140.1. LRMS (ES^+) *m/z*: 220.1 $[M+H]^+$. HRMS (ES^+) calcd. for $C_{13}H_{15}NCl$ $[M+H]^+$ 220.0893, found 220.0892.

Methyl 5-chloro-2,3,4,9-tetrahydro-1H-carbazole-1-carboxylate (21)

General Fischer indole procedure with 3-chlorophenylhydrazine hydrochloride (482.3 mg, 2.69 mmol) and methyl-2-oxocyclohexane-1-carboxylate (459.7 mg, 2.94 mmol) in glacial acetic acid (4 mL) provided **21** (32.9 mg, 5% yield) as a pale yellow oil following FCC on silica gel (1:1:98 Et_2O/EtOAc/petrol)**.** ^{1}H NMR ($CDCl_3$, 300 MHz): 1.82-1.88 (1H, m), 2.02-2.07 (1H, m), 2.15-2.23 (3H, m), 3.79 (3H, s), 3.87 (1H, t, *J* = 6.3Hz), 7.00 (1H, t, *J* = 7.8 Hz), 7.15 (1H, d, *J* = 7.5 Hz), 7.37 (1H, d, *J* = 7.8 Hz), 8.50 (1H, s). ^{13}C NMR ($CDCl_3$, 75 MHz): 20.9, 21.7, 26.1, 39.9, 52.5, 113.2, 116.4, 117.0, 120.2, 121.4, 128.9, 130.4, 133.3, 172.9. LRMS (ES^-) *m/z*: 262.05 $[M-H]^-$. HRMS (ESI^-) calcd. for $C_{14}H_{13}NO_2Cl$. 262.0635, found 262.0645.

8-chloro-2,3,4,9-tetrahydro-1H-carbazole (22)[13]

General Fischer indole procedure with 2-chlorophenylhydrazine hydrochloride (258.8 mg, 1.45 mmol) and cyclohexanone (162.8 mg, 1.66 mmol) in glacial acetic acid (4 mL) provided **22** (129.4 mg, 43% yield) as a pale yellow oil following FCC on silica gel (1:9 – 2:8 Et_2O/petrol). ^{1}H NMR (MeOD, 500 MHz): 1.85-1.90 (4H, m) 3.64-2.66 (2H, t like), 2.74-2.76 (2H, t like), 6.89 (1H, t, *J* = 7.8 Hz,), 6.98 (1H, d, *J* = 7.5 Hz), 7.26 (1H, d, *J* = 8.0 Hz). ^{13}C NMR (MeOD, 125MHz): 22.0, 24.0, 24.3, 23.5, 111.0, 116.9, 117.0, 120.0, 120.7, 130.9, 134.4, 136.8. LRMS (ES^-) m/z: 205 $[M-H]^-$. LRMS (ES^-) m/z: 205 $[M-H]^-$. HRMS ($ASAP^+$) calcd. for $C_{12}H_{13}NCl$ $[M+H]^+$ 206.0737, found 206.0739.

8-chloro-2,3,4,9-tetrahydro-1H-carbazole-3-carboxylic acid (24)[14]

General deesterification procedure with **23** (77.0 mg, 0.28 mmol) provided **24** (21.5 mg, 31% yield) as an off-white powder following FCC on silica gel (20:80:0.5 EtOAc/petrol/acetic acid), mp 196 -198 °C. ^{1}H NMR (MeOD, 500 MHz): 1.97-2.00 (1H, m), 2.27-2.30 (1H, m), 2.78-2.87 (4H, m,), 2.97-3.01 (1H, m), 6.91 (1H, t, *J* = 7.8 Hz), 7.01 (1H, d, *J* = 8.0 Hz), 7.29 (1H, d, *J* = 8.0 Hz). ^{13}C NMR (MeOD, 125 MHz): 23.1, 25.0, 27.0, 41.5, 109.3, 117.0, 120.3, 121.0, 130.6, 134.7, 136.1, 179.4. LRMS (ES^-) *m/z*: 248.15 $[M-H]^-$. HRMS (ES^-) calcd. for $C_{13}H_{11}NO_2Cl$ $[M-H]^-$ 248.0478, found 248.0477.

6-chloro-2,3,4,9-tetrahydro-1H-carbazol-7-ol (25)

General hydrazine formation procedure with 2-chloro-5-aminophenol (1.93 g, 13.45 mmol) provided 2-chloro-5-hydrazinylphenol hydrochloride (**30**; 1.99 mg, 75% yield) as a pinkish powder, mp >160 °C (dec.). ^{1}H NMR (d_6-DMSO, 500 MHz): 6.42 (1H, dd, *J* = 8.5, 2.5 Hz), 6.60 (1H, d, *J* = 2.0 Hz), 7.20 (1H, d, 8.5 Hz), 8.23 (1H, s), 10.06 (1H, br s), 10.25 (1H, s). LRMS (ES^+) m/z: 159.04 $[M+H]^+$.

General Fischer indole procedure with **30** (528.7 mg, 2.71 mmol) and cyclohexanone (285.3 mg, 2.90 mmol) in absolute ethanol (6 mL) provided **25** (16.7 mg, 8% yield) as a beige powder following FCC on silica gel (gradient elution; 1:9-4:6 Et_2O/petrol), mp 150 – 152 °C. ^{1}H NMR ($CDCl_3$, 500 MHz): 1.84-1.88 (4H, m), 2.60-2.62 (2H, m), 2.65-2.67 (2H, m), 6.90 (1H, s), 7.35

(1H, s), 7.54 (1H, s). ^{13}C NMR ($CDCl_3$, 125 MHz): 20.9, 23.2, 23.3, 97.3, 109.8, 113.1, 117.3, 123.1, 134.3, 135.5, 146.4. LRMS (ES^+) *m/z*: 221.89 $[M+H]^+$. HRMS ($ASAP^+$) calcd. for $C_{12}H_{13}NOCl$ $[M+H]^+$ 222.0686, found 222.0676.

6-chloro-2,3,4,9-tetrahydrocarbazole-2,5-dicarboxylic acid (26)

General Fischer indole procedure with 2-chloro-5-hydrazinobenzoic acid hydrochloride (**32**; 196.5 mg, 0.88 mmol) and 3-oxocyclohexanecarboxylic acid (117.4 mg, 0.83 mmol) in glacial acetic acid (2 mL) produced a mixture of two isomers. The desired isomer was separated by first methylating the mixture (general esterification procedure), followed by FCC on silica gel (40:60:0.5 EtOAc/petrol/acetic acid) to give the mono-methylated 6-chloro-2,3,4,9-tetrahydrocarbazole-2,5-dicarboxylic acid (48.5 mg), which was demethylated (general deesterification procedure) to give **26** (15.6 mg, 10% yield) as a pale yellow powder, mp 222 – 224 °C. ^{1}H NMR (MeOD, 500 MHz): 1.89-1.94 (1H, m), 2.24-2.66 (1H, m), 2.66-2.72 (1H, m), 2.77-2.87 (2H, m), 2.98-3.00 (2H, m), 7.03 (1H, d, *J* = 8.0 Hz), 7.27 (1H, d, *J* = 9.0 Hz). ^{13}C NMR ($CDCl_3$+MeOD, 125 MHz): 20.4, 25.4, 26.3, 39.6, 107.7, 112.6, 120.4, 121.1, 123.6, 124.4, 134.9, 135.5, 179.0. LRMS (ES^+) *m/z*: 316.15 $[M+Na]^+$. HRMS (ES^+) calcd. for $C_{14}H_{12}NO_4ClNa$ $[M+Na]^+$ 316.0353, found 316.0348.

7-chloro-1,2,3,4-tetrahydrocyclopenta[b]indole-8-carboxylic acid (27)

General Fischer indole procedure with 2-chloro-5-hydrazinobenzoic acid hydrochloride (**32**; 436.2 mg, 1.96 mmol) and cyclopentanone (139.6 mg, 1.66 mmol) in glacial acetic acid (2 mL) provided **27** (11.3 mg, 2% yield) as a yellow powder following FCC on silica gel (30:70:0.5 EtOAc/petrol/acetic acid) and recrystallisation from methanol/water, mp 208 – 210 °C. ^{1}H NMR (d_6-DMSO, 300 MHz): 2.40-2.44 (2H, m), 2.68 (2H, br t, *J* = 6.8 Hz), 2.82 (2H, br t, *J* = 7.2Hz), 7.01 (1H, d, *J* = 9 Hz), 7.34 (1H, dd, *J* = 8.7, 1.2 Hz), 11.26 (1H, s), 13.17 (1H, s). ^{13}C NMR (d_6-DMSO, 75 MHz): 24.9, 25.2, 28.0, 114.1, 117.2, 120.1, 120.2 (C-H), 122.7 (2xC), 139.5, 147.6, 167.8. LRMS (ES^-) m/*z*: 234.0 $[M-H]^-$. HRMS (ES^-) calcd. for $C_{12}H_9NO_2Cl$ $[M-H]^-$ 234.0322, found 234.0320.

Methyl 6-chloro-2,3,4,9-tetrahydrocarbazole-7-carboxylate (29)

General Fischer indole procedure with 2-chloro-5-hydrazinobenzoic acid hydrochloride (**32**; 364.5 mg, 1.63 mmol) and cyclohexanone (113.3 mg, 1.15 mmol) in glacial acetic acid (4 mL) provided 6-chloro-2,3,4,9-tetrahydrocarbazole-7-carboxylic acid (44.4 mg, 16% yield) as a white powder following FCC on silica gel (20:80:0.5 EtOAc/petrol/acetic acid). ^{1}H NMR ($CDCl_3$ + d_6-DMSO, 500 MHz): 1.87-1.91 (4H, m), 2.66-2.67 (2H, m), 2.75-2.76 (2H, m), 7.43 (1H, s), 7.98 (1H, s), 9.79 (1H, s). LRMS (ES^+) *m/z*: 272.2 $[M+Na]^+$. HRMS (ES^+) calcd. for $C_{13}H_{13}NO_2Cl$ $[M+H]^+$ 250.0635, found 250.0657.

General esterification procedure with 6-chloro-2,3,4,9-tetrahydrocarbazole-7-carboxylic acid (36.6 mg, 0.15 mmol) in methanol (1.5 mL) provided **29** (7.0 mg, 18% yield) as a beige powder following trituration with CH_2Cl_2, mp 198 -200 °C. ^{1}H NMR (d_6-DMSO, 500 MHz): 1.77-1.83 (4H, m), 2.59-2.61 (2H, m), 2.72-2.73 (2H, m), 3.82 (3H, s), 7.46 (1H, s), 7.79 (1H, s), 11.19 (1H, br s). ^{13}C NMR (d_6-DMSO, 125 MHz): 20.3, 22.4, 22.6, 22.8, 51.9, 108.8, 114.1, 118.8, 119.7, 121.9, 130.4, 133.2, 140.5, 166.1. LRMS (ES^+) *m/z*: 286.211 $[M+Na]^+$. HRMS (ES^+) calcd. for $C_{14}H_{15}NO_2Cl$ $[M+H]^+$ 264.0791, found 264.0800.

Supplementary References

(1) Georgescu, R. E.; Yurieva, O.; Kim, S. S.; Kuriyan, J.; Kong, X. P.; O'Donnell, M. Structure of a small-molecule inhibitor of a DNA polymerase sliding clamp. *Proc. Nat. Acad. Sci. U.S. A.* **2008**, 105, 11116-11121.
(2) Wijffels, G.; Johnson, W. M.; Oakley, A. J.; Turner, K.; Epa, V. C.; Briscoe, S. J.; Polley, M.; Liepa, A. J.; Hofmann, A.; Buchardt, J.; Christensen, C.; Prosselkov, P.; Dalrymple, B. P.; Alewood, P. F.; Jennings, P. A.; Dixon, N. E.; Winkler, D. A. Binding inhibitors of the bacterial sliding clamp by design. *J. Med. Chem.* **2011**, 54, 4831-4838.
(3) Irwin, J. J.; Sterling, T.; Mysinger, M. M.; Bolstad, E. S.; Coleman, R. G. ZINC: A Free Tool to Discover Chemistry for Biology. *J. Chem. Inf. Model* **2012**.
(4) Lang, P. T.; Moustakas, D.; Brozell, S.; Carrascal, N.; Mukherjee, S.; Pegg, S.; Raha, K.; Shivakumar, D.; Rizzo, R.; Case, D.; Shoichet, B.; Kuntz., I. *DOCK, Version 6.2*, 2008.
(5) Graves, A. P.; Shivakumar, D. M.; Boyce, S. E.; Jacobson, M. P.; Case, D. A.; Shoichet, B. K. Rescoring docking hit lists for model cavity sites: predictions and experimental testing. *J. Mol. Biol.* **2008**, 377, 914-934.
(6) Mortenson, P. N.; Murray, C. W. Assessing the lipophilicity of fragments and early hits. *J. Comput. Aided Mol. Des.* **2011**, 25, 663-667.
(7) Green, N. J.; Xiang, J.; Chen, J.; Chen, L.; Davies, A. M.; Erbe, D.; Tam, S.; Tobin, J. F. Structure–activity studies of a series of dipyrazolo[3,4-b:3′,4′-d]pyridin-3-ones binding to the immune regulatory protein B7.1. *Bioorganic & Med. Chem.* **2003**, 11, 2991-3013.
(8) Macdonald, J. E.; Jackson, A. J.; Mittapalli, G. K.; Zhao, F.; Rijnbrand, C. A.; Lee, H.; Zhang, J.; Wong-Stall, F. Derivatives of substituted fused ring cycloindoles and methods of their use. WO 2009103022, 20 August, 2009.
(9) Sneddon, S. F.; Beskrovnaya, O.; Gregory, J. S.; Smith, L. A.; Husson, H.; Bukanov, N. O.; Yee, C.; Hirth, B. H.; Cuff, L. M.; Janjigian, A.; Bastos, C. M.; Hilmy, A.; Skell, J.; Giragossian, C.; Cochran, B.; Serrano, M. A method for treating polycystic kidney disease using 3-hydroxymethyl-substituted carbazole and related derivatives. WO 2006012310, 2 February, 2006.
(10) Miyata, O.; Takeda, N.; Kimura, Y.; Takemoto, Y.; Tohnai, N.; Miyata, M.; Naito, T. Efficient synthesis of indoles using [3,3]-sigmatropic rearrangement of N-trifluoroacetyl enehydrazines. *Tetrahedron* **2006**, 62, 3629-3647.
(11) Johnson, R. P.; Oswald, J. P. Ardylalkyl derivatives of 1,2,3,4-tetrahydro-5H-pyrido[4,3b]indoles. US 3382250, 7 December, 1968.
(12) Rice, L. M.; Hertz, E.; Freed, M. E. Antidepressant agents. Derivatives of 2,3-polymethyleneindoles. *J. Med. Chem.* **1964**, 7, 313-319.
(13) Chen, J.; Hu, Y. Microwave-Assisted One-Pot Synthesis of 1,2,3,4-Tetrahydrocarbazoles. *Synthetic Commun.s* **2006**, 36, 1485-1494.
(14) Robinson, F. P.; Brown, R. K. Further evidence for the dienone-imine intermediate in the Fischer indole synthesis. An uncatalyzed Fischer reaction under mild conditions. *Can. J. of Chem.* **1964**, 42, 1940-1947.